Dynamic Carboniferous climate change, Arrow Canyon, Nevada

James W. Bishop*
Isabel P. Montañez
David A. Osleger
Geology Department, University of California–Davis, Shields Avenue, Davis, California 95616, USA

ABSTRACT

The Phanerozoic's longest-lived and most widespread glaciation, the late Paleozoic ice age, is undergoing a resurgence in interest. Long-held models of the timing, duration, and magnitude of glaciation are being reevaluated due to emerging evidence from former high latitudes, evidence that the late Paleozoic ice age was punctuated by long-lived glacial minima or possibly ice-free times.

The history of the late Paleozoic ice age is archived within the biostratigraphically well-constrained, carbonate-dominated succession of Arrow Canyon, Nevada, United States. In this paleo-tropical succession, the distribution of lithofacies, flooding surfaces, and subaerial exposure horizons and their stacking into meter-scale cycles record a detailed climate history. The onset of this phase of glaciation during the middle Mississippian was followed by a dynamic evolution of glacioeustasy through the late Mississippian to late Pennsylvanian. Moderate- to high-amplitude glacioeustasy was likely interrupted by an earliest Pennsylvanian short-lived glacial minimum, but otherwise appears to have persisted through the middle Pennsylvanian.

Upper Pennsylvanian strata record low- to moderate-amplitude relative sea-level changes, suggesting a long-lived interval of diminished ice volume. This proposed glacial minimum is coincident with a notable minimum in glaciogenic sedimentation near the former southern pole, aridification across paleo-tropical Pangea, and significant floral and faunal turnover, suggesting a link between tropical environmental change and high-latitude glaciation. These conclusions, however, are at odds with those traditionally inferred from Euramerican cyclothems, i.e., persistent high-amplitude glacioeustasy driven by a single, large ice sheet. Rather, the Arrow Canyon archive of varying depositional facies and cycle stacking patterns records major changes in the magnitude of short-term glacioeustasy. This finding contributes to recent and growing near- and far-field evidence for a more dynamic glaciation history than previously inferred from the classic Euramerican cyclothems.

INTRODUCTION

Much of our understanding of the late Paleozoic ice age (LPIA) has been built on stratigraphic records from the low-latitude tropics, typified by Euramerican cyclothems. These far-field records preserve high-frequency sequences of open-marine, paralic, and terrestrial environments. Cyclothems have long been considered the most sensitive proxy of high-frequency (10^5 yr) glacioeustasy, driven by the waxing and waning of expansive ice sheets in Southern Hemisphere Gondwana (e.g., Wanless and Weller, 1932; Wanless and Shepard, 1936; Heckel, 1977). The persistence of cyclothems in upper Mississippian through lower Permian successions has been argued as evidence for repeated short-term (20–400 k.y.), high-amplitude (30 to >150 m) sea-level changes, and in turn the persistence of large-scale continental glaciation throughout an ~50 m.y period of the Carboniferous–Permian (Heckel, 1977, 1986, 1994, 2002; Veevers and Powell, 1987; Horbury, 1989; Frakes et al., 1992; Soreghan and Giles, 1999a; Smith and Read, 2000; Cook et al., 2002; Zempolich et al., 2002; Heckel et al., 2007).

This paradigm has been challenged by emerging near-field records. In particular, recent compilations of paleo–high-latitude Gondwanan records document discreet intervals of widespread glaciogenic sedimentation, punctuated by periods of normal marine or fluviodeltaic sedimentation, or long-lived pedogenesis (e.g., Isbell et al., 2003a, 2003b, 2008a, 2008b; Fielding et al., 2008a, 2008b, 2008c, and references therein). These records argue for intervals of glacial minima during the late Paleozoic ice age, with geographically restricted ice centers or possibly ice-free conditions near the South Pole for periods of several million years. This conclusion calls into question how fluctuating continental ice sheets could have sustained large (>50 m) sea-level changes throughout the late Paleozoic. Moreover, recent studies of some far-field cyclothem records also suggest varying characteristics of cyclothems, with intervals of potential lower amplitude glacioeustatic forcing (e.g., West et al., 1997; Smith and Read, 2000; Wright and Vanstone, 2001; Gibling and Giles, 2005; Heckel, 2008). Accordingly, climate simulations indicate that the response of ice sheets to orbital forcing was quite sensitive to variations in pCO_2 and overall ice sheet size, leading to a range of possible glacioeustatic magnitudes (Horton et al., 2007). Thus, changes in the frequency and amplitude of Carboniferous–Permian glacioeustasy should be expected during the course of the late Paleozoic ice age if the extent and volume of stable continental ice sheets varied. This hypothesis, however, has been minimally tested in the low-latitude paleo-tropical basins.

This study documents lithologic, pedogenic, and early diagenetic facies and their stratigraphic stacking into meter-scale cycles in the Carboniferous succession of Arrow Canyon, Nevada, United States. This carbonate-dominated succession has nearly complete exposure, relatively high subsidence rates, and a very well constrained biostratigraphy; in addition, carbonates tend to fill accommodation space and are thus highly sensitive to climate change and siliciclastic input. Our approach is to use the changes in facies and cycle types to reconstruct ~30 m.y. of Carboniferous relative sea-level and climate history on the paleo-tropical western margin of Euramerica. Though we show that the long-term

*Present address: Chevron Energy Technology Company, 6001 Bollinger Canyon Road, C-1217, San Ramon, California 94583, USA; James.Bishop@Chevron.com.

Geosphere; February 2010; v. 6; no. 1; p. 1–34; doi: 10.1130/GES00192.1; 17 figures; 4 tables.

accommodation record is dominated by subsidence variations, the short-term high-amplitude relative sea-level record is inferred to reflect the repeated waxing and waning of Gondwanan ice sheets. A tectonic explanation for such moderate- to high-amplitude relative sea-level changes is ruled out by their character, longevity, bounding surfaces, and the record of coeval glaciogenic sediments in high latitudes. Thus, the presence and magnitude of such short-term changes are taken as proxy for minimum possible ice volume (cf. Read, 1995; Smith and Read, 2000; Wright and Vanstone, 2001). In particular, in this paper we note the absence of such moderate- to high-amplitude relative sea-level changes during intervals traditionally ascribed to peak glacioeustasy (e.g., late Pennsylvanian), an absence that cannot be explained by tectonic drivers. Because the lack of high-amplitude glacioeustasy might be due to small ice sheets or the presence of a very large, stable ice sheet (DeConto and Pollard, 2003; Horton et al., 2007), we look to the high-latitude record of glaciogenic sedimentation to distinguish large, stable ice sheets from small, feckless ones.

Different climate modes are suggested for the Arrow Canyon succession by changes in patterns of meter-scale cyclicity and facies distributions. These changes delineate intervals of distinct short-term relative sea-level fluctuations and regional climate. These intervals are ultimately linked to changing glaciation by ties between ice volume and eustasy (e.g., Read, 1995; Smith and Read, 2000), and between continental ice sheets and low-latitude precipitation (Cecil et al., 2003; Poulsen et al., 2007). The Arrow Canyon succession records the onset of glacioeustasy in basal Chesterian time, a short-lived glacial minimum in earliest Morrowan time, and a long-lived, significantly drier glacial minimum during later Desmoinesian through early Virgilian time.

TECTONIC AND GEOLOGIC SETTING

The Arrow Canyon Range is in southeastern Nevada, in the eastern Great Basin province. During the middle to late Paleozoic, Arrow Canyon was situated in the tropics on the west coast of the North American craton, near the seaward margin of an interior seaway that at times extended from California to Alaska (Poole and Sandberg, 1991; Ross, 1991) (Fig. 1). Southeastern Nevada was in the foreland basin inherited from the Devonian–early Mississippian Antler orogeny (Dickinson, 2006). During middle Mississippian to early Permian time, the former foreland evolved as a series of basins and uplifts. Tectonic controls on this structural landscape are not well constrained and may relate to distal effects of the Ouachita-Marathon orogeny and thus be linked to the Ancestral Rocky Mountains (Kluth and Coney, 1981; Kluth, 1986; Dickinson, 2006). Alternatively, they may relate to a continuing post-Antler tectonic evolution of the western margin of North America (Trexler et al., 1991, 2003, 2004; Stevens and Stone, 2007).

Platform geometries evolved during the course of Carboniferous sedimentation. We use "platform" in the sense of Read (1985) to encompass both ramps and shelves. Middle to late Mississippian Arrow Canyon strata accumulated on a carbonate or mixed carbonate-siliciclastic ramp, with correlative basinal facies to the west in western Nevada and Death Valley (Stevens et al., 1991; Poole and Sandberg, 1991; Trexler et al., 1996). During Pennsylvanian time, the study area was on the northeast Bird Spring platform of the Keeler Basin (also known as Bird Spring Basin; Kluth, 1986) that initiated as a ramp during the early Pennsylvanian (Morrowan; Stevens et al., 1991, 2001; Stevens and Stone, 2007) but evolved into an attached shelf by late Pennsylvanian time. During Morrowan, Atokan, and possibly early Desmoinesian time, the Bird Spring platform was a distally steepened ramp, indicated by rare sediment gravity flows in the basin (Yose and Heller, 1989; Miller and Heller; 1994), unrestricted storm-dominated strata in Arrow Canyon, and the absence of evidence for any margin (e.g., biohermal buildups or grainstone shoal complexes at a break in slope). By contrast, in upper Desmoinesian through Wolfcampian time, the Bird Spring platform prograded westward and evolved into a (locally) rimmed shelf, as evidenced by abundant turbidites, debris flows, and megabreccias in basinal settings (Yose and Heller, 1989; Miller and Heller; 1994), restricted platform interior facies in Arrow Canyon, and phyloid algal bioherms with bypass channels, which mark the shelf margin in the Nevada Test Site and Death Valley (Miller and Heller, 1994; Stevens et al., 2001).

Nearly continuous, high subsidence in the Arrow Canyon region promoted a thick, relatively stratigraphically complete Carboniferous succession. Long-term (second- to third-order) accommodation in this setting was driven by regional tectonics; however, this study examines the high-frequency stratigraphic record to extract climatic signatures during the Carboniferous interval. Most of the succeeding Permian and Mesozoic strata were removed by a regional unconformity caused by the Cretaceous Sevier orogeny (Page and Dixon, 1997). During Neogene time, basin and range extension uplifted the Arrow Canyon Range in a north-south–trending block, and canyons cutting through the range now expose a nearly complete Famennian to Wolfcampian carbonate-dominated succession.

METHODOLOGY AND CHRONOSTRATIGRAPHY

A composite section was measured on both sides of Arrow Canyon, encompassing Osagean through lower Virgilian (Visean through Gzhelian Russian Platform stages) strata of the Yellowpine, Battleship Wash, Indian Springs, and Bird Spring Formations. Upper Virgilian and Wolfcampian strata are heavily recrystallized, obscuring many depositional and early diagenetic features; these strata are not discussed here. Above the base of the Indian Springs Formation, the section was tied to a standard canyon section, measured by Amoco Oil Company as part of an extensive biostratigraphic research program in Arrow Canyon, and along which brass tags and metal spikes were affixed every 1.5 m (stratigraphic locations in this paper are labeled with an "A" prefix, corresponding to this standard measured section). To refine lithofacies interpretations, identify faunal assemblages, and describe early diagenetic features, 663 samples were collected, thin-sectioned, stained with Alzarin red and potassium ferricyanide (Dickson, 1965), and examined under transmitted and cathodoluminescent light.

Biostratigraphic control is provided by conodonts, calcareous algae, foraminifera, and fusulinids (Appendix A). The thick, relatively complete Arrow Canyon succession includes the Global Stratotype Section and Point for the Mississippian-Pennsylvanian boundary (Brenckle et al., 1997; Lane et al., 1999; Richards et al., 2002; Ellwood et al., 2007; Barnett and Wright, 2008; Bishop et al., 2009), and has been a focus of biostratigraphic research for nearly 50 yr (Cassity and Langenheim, 1966; Webster, 1969; Pierce and Langenheim, 1972; Rice and Langenheim, 1974a, 1974b; Langenheim et al., 1984; Baesemann and Lane, 1985; Brenckle, 1997; Stamm and Wardlaw, 2003). Chronostratigraphy for this study is based primarily on extensive Amoco biostratigraphic data, collected over several decades, and subsequently donated to the Universities of Iowa (conodonts) and Kansas (foraminifera) (Groves and Miller, 2000). This biostratigraphic control begins below the Osagean Yellowpine Formation and continues through the Chesterian to lower Wolfcampian Bird Spring Formation. Many of the range charts and original thin sections have since been reinterpreted (Leavitt, 2002; Vladimir Davydov, 2007, personal commun.; Greg Wahlman, 2006–2007, personal communs.; Bishop et al., 2009) and are used here. Appendix A presents the preferred biostratigraphic zonation tied to meterage,

A numbers, and the bed numbers of Cassity and Langenheim (1966) where appropriate.

LITHOFACIES AND DEPOSITIONAL ENVIRONMENTS

Carboniferous strata in the study area were deposited on a westward-facing platform that we divide into broad depositional settings: outer, middle, and inner ramp (Mississippian to middle Pennsylvanian) and shelf interior (upper Pennsylvanian). Lithofacies descriptions for each are provided in Tables 1–4. In the following we highlight salient features of each setting and offer an environmental interpretation. Lithofacies are defined and interpreted using their Dunham textures, sedimentary structures, and photozoan versus heterozoan grain types. Heterozoan fossil assemblages consist primarily of echinoderms, bryozoa, brachiopods, foraminifera, solitary corals, calcareous red algae, sponge spicules, and trilobites. Photozoan assemblages consist primarily of coated grains, peloidal lime mud, fully micritized grains,

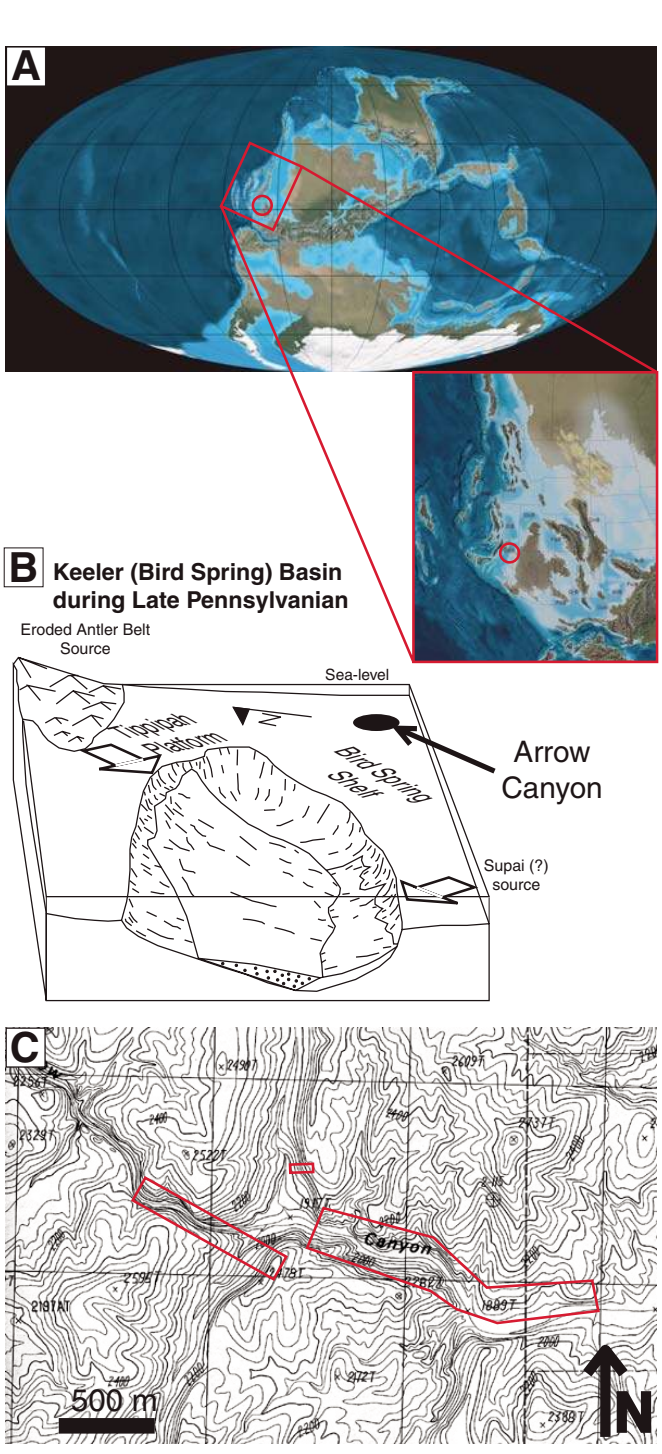

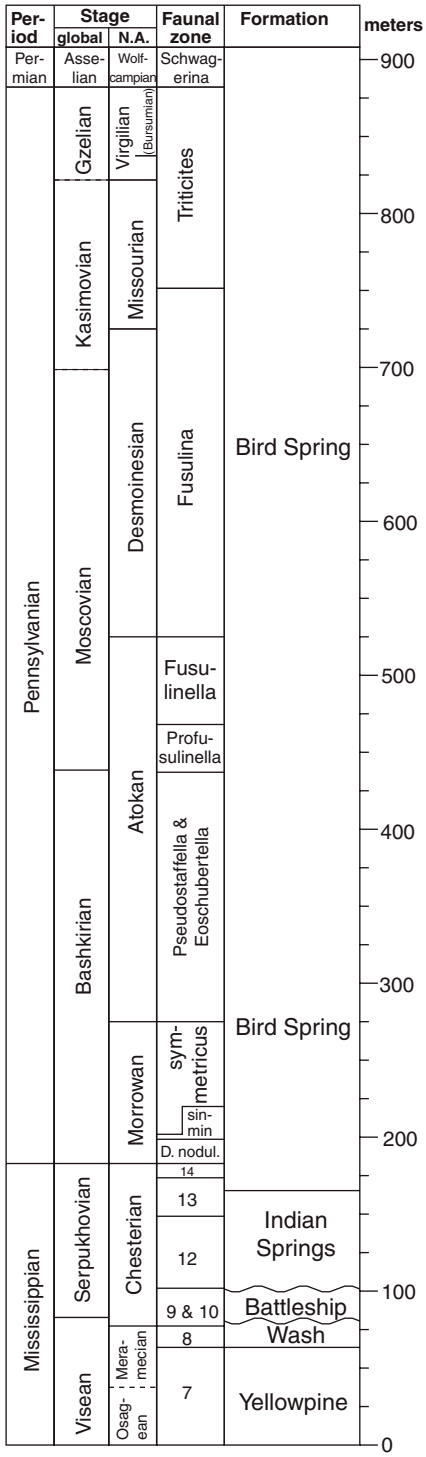

Figure 1. (A) Middle Pennsylvanian paleogeography (after Blakey, 2007). Circle indicates Arrow Canyon, within 10° of the equator. Inset shows Missourian paleogeography of western North America. (B) Late Pennsylvanian schematic of the Keeler–Bird Spring Basin, with Arrow Canyon positioned on the Bird Spring shelf (after Miller and Heller, 1994). (C) Topographic map showing the location of sections measured in Arrow Canyon (USGS, 1986). (D) Biostratigraphic zonation for Arrow Canyon, compiled from Appendix A.

TABLE 1. OUTER-RAMP FACIES

Facies	Bedding and color	Sedimentary structures	Lithology	Components		Depositional environment	Water depth
				Biotic	Abiotic		
Marl (OR1)	Massive to nodular; chalky, gray, black to purple on fresh surface	Millimeter to centimeter lamination defined by thin insoluble-rich seams	Argillaceous, silty lime mudstone to wackestone, locally dolomitized	Mostly unidentifiable silt-sized bioclasts; locally common whole brachiopod valves and shells, articulated echinoderm columnals, and solitary corals	Silt-sized peloids; common euhedral pyrite and carbonate-cemented nodules	Deep subtidal, below SWB, dysoxic pore waters	>50 (c)
Wavy interbedded calcisiltite and chert (OR2)	Decimeter-scale wavy beds; blue-gray limestone with black chert	Millimeter lamination, minor bioturbation. Nodular to wavy bedded chert	Recrystallized chert with little texture, spiculitic calcisilt, locally dolomitized	Unidentifiable silt-sized bioclasts; common calcite-filled molds after spicules, thin-walled brachiopods, bryozoa, articulated crinoid columnals, solitary corals	Silt-sized peloids	Near to below SWB, likely bathed by upwelling waters	>40 (c)
Massive to laminated calcisiltite (OR3)	Massive to decimeter scale; blue-gray	Local millimeter lamination, minor bioturbation	Calcisilt, locally dolomitized	Unidentifiable silt-sized bioclasts; common calcite-filled molds after spicules; locally common thin-walled brachiopods, bryozoa, articulated echinoderm columnals, solitary corals	Silt-sized peloids	Proximal to or below SWB	40–70 (c)
Laminated siltstone and mudstone (OR4)	Red to yellow to brown, blue-gray to black on fresh surface	Even to discontinuous millimeter lamination, lightly burrowed	Quartz silt, mica, clay	Rare brachiopod, crinoid ossicle	N/A	Below FWWB and locally SWB, prodelta or lower shoreface to offshore	20–60 (b, c)

Note: Outer-ramp facies. Parenthetical letters after water depth range correspond with (b) between FWWB and storm wave base, SWB, and (c) below SWB.

TABLE 2. MID-RAMP FACIES

Facies	Bedding and color	Sedimentary structures	Lithology	Component		Depositional environment	Water depth (m)
				Biotic	Abiotic		
Cross-stratified calcisiltite (MR5)	Centimeter to decimeter scale; blue-gray	Low-angle truncation, rare current and/or wave-ripples	Calcisiltite	Unidentifiable silt-sized bioclasts; common calcite-filled molds after sponge spicules	Silt-sized peloids	Near to above SWB	35–40 (b)
Offshore heterozoan W/P (MR6)	Centimeter to decimeter to meter scale; gray	Typically thoroughly bioturbated; locally mm-scale grainy and muddy laminations	Lime wackestone to packstone, locally partially dolomitized	Common echinoderms, bryozoa, spicule molds, brachiopods (spines), trilobites, solitary corals, forams, rare red algae and mollusks	Rare glendonite pseudomorphs after ikaite	Between FWWB and SWB	15–40 (b)
Offshore photozoan W/P (MR7)	Decimeter to meter scale; gray to tan	Well-burrowed grainy and muddy laminations	Wackestone to packstone	Common whole brachiopod valves and shells, forams, fusulinids, bryozoa, solitary corals trilobites and articulated echinoderms, rare sponge spicules	Coated grains, locally peloidal	Seaward of skeletal and/or coated grain banks and shoals, from FWWB to SWB	15–30 (b, d)

Note: SWB—storm wave base; FWWB—fair weather wave base; W/P—wacke-packstone. (b) Between FWWB and SWB; (d) within photic zone.

TABLE 3. INNER-RAMP FACIES

Facies	Bedding and color	Sedimentary structures	Lithology	Component		Depositional environment	Water depth (m)
				Biotic	Abiotic		
Cross-stratified sandstone (IR8)	Centimeter to meter scale; red to yellow to gray	Planar tabular to trough cross-stratified, rare current and/or wave ripples	Silt to medium sand sized quartz	None	Hematite staining common	Marine; middle to upper shoreface	1-20 (a)
Heterozoan G/P (IR9)	Decimeter to meter scale; blue, gray	Typically bioturbated, local planar-tabular and rarely trough cross-stratification	Lime grainstone to packstone	Echinoderms, bryozoa, brachiopods (spines), spicules, trilobites, solitary corals, forams, rare mollusks and coralline red algae	None	Shoals and skeletal banks near to above FWWB	5-20 (a, e, g)
Photozoan G/P (IR10)	Centimeter to meter scale; blue, gray, tan	Planar tabular cross-stratification common, rare wave ripples	Local cauliflower chert nodules	Fusulinids, *Syringapora* coral heads, brachiopods, bryozoa, solitary corals, echinoderms, forams, trilobites,	Common oolitic, oncolitic coatings, micritized sand-sized peloids; local cauliflower chert	Shoals and shorelines near to above FWWB	5-20 (a, e, g)
Thrombolite (IR10b)	Decimeter scale beds; blue	Micritic thrombolite, 1-5 cm diameter, <30 cm high, unknown synoptic relief; quartz and lime sand in troughs	Boundstone and grainstone	Abundant forams (commonly encrusting) common mollusks,	Clotted micrite, coated grains, fully micritized grains, peloids	Shallow subtidal, photic, swept by currents	1-5 (j)
Metazoan framestone (IR10c)	Massive; tan	Decimeter to meter diameter bioherms and biostromes	Framestone, variably dolomitized	Tabulate (*Syringapora*) and colonial rugose (*Siphonodendron, Cystolonsdaleia*) corals, Chaetetes, matrix similar to IR10, IR12, or MR7)	Peloids, coated grains, fully micritized grains	Shallow subtidal, above FWWB, bioherms may baffle mud	<1-15 (a)
Coated G/P (IR10d)	Decimeter to meter scale; blue-gray to tan	Planar tabular to trough cross-stratified	Grainstone to packstone	Mostly as nuclei: fusulinids, coral fragments, brachiopods, bryozoa, echinoderms, forams, trilobites	Oncolitic to oolitic cortices; local cauliflower chert anhydrite pseudomorphs	Shallow, wave-washed shoals and shorelines, above FWWB	0-5 (a, d, g, h, i)
Lagoonal heterozoan W/P (IR11)	Centimeter to meter scale; gray	Thoroughly bioturbated	Wackestone to packstone, variable dolomite	Common whole brachiopod valves and shells, articulated crinoid stems, solitary corals; bryozoa fronds, muddy matrix	Common silt-sized peloids	Lagoonal (positioned between shoals and tidal flats)	2-20 (a, e)
Lagoonal photozoan W/P (IR12)	Decimeter to meter scale or massive; gray to tan	Typically thoroughly bioturbated, local grainy traction deposits	Wackestone and packstone, variable dolomite, chert nodules	Common whole brachiopod valves and shells, forams, fusulinids, bryozoa, solitary corals trilobites and articulated echinoderms; mollusk molds; rare chaetetes, sponges and Syringapora coral heads	Peloidal matrix, common oncolitic coatings, rare oolitic coatings, thick micrite envelopes	Evaporative lagoon	2-20 (a, e)
Dolomitized photozoan W/P (IR12b)	Decimeter to meter scale or massive; tan	Typically thoroughly bioturbated, local grainy traction deposits	Dolowackestone and packstone, variably cherty	Common large fusulinids, brachiopods (spines), bryozoa, crinoids	Abundant peloids; common cauliflower chert pseudomorphs after anhydrite	Shallow, highly restricted, evaporative lagoon	2-5 (a, e)
Laminite (IR13)	Centimeter to decimeter scale; tan, locally blue	Planar millimeter to centimeter laminations of mud and peloids/skeletal grains, fenestrae, mudcracks, crinkly with LLH stromatolites, cut and fill structures	Dolomudstone, wackestone, and packstone	Brachiopods (spines), trilobites; rare bryozoa, fusulinids	Peloids, coated grains; common cauliflower chert pseudomorphs after anhydrite	Intertidal to supratidal; cryptmicrobial laminites	0-2 (k)
Paleosol (IR14)	Centimeter to meter scale; yellow-red-brown	Roots, glaebules, circum-granular cracks, soil pisoids; ped structure, horizonation, slickensides	Calcisols, Protosols, Argilisols, and Vertisols	Those of overprinted limestone facies; rhizoliths and redoximorphic root haloes	Soil pisoids	Soil	0 (l)
Calcareous sandstone (IR15)	Centimeter to decimeter scale; yellow-red	Massive, rarely even millimeter to centimeter “pinstripe” cross-lamination	Quartz sand and silt	Rarely, rhizoliths	Quartz silt to very fine sand	Eolian, reworked during transgressions	0 (l)

Note: G/P—pack-grainstone; W/P—wacke-packstone; FWWB—fair weather wave base. (a) Above FWWB, (d) within photic zone, (e) Purser and Evans (1973), (f) Logan et al. (1970), (g) Hagan and Logan (1974), (h) Loreau and Purser (1973), (i) Harris (1979), (j) Osleger and Read (1991), (k) intertidal, and (l) supratidal.

TABLE 4. SHELF INTERIOR FACIES

Facies	Bedding and color	Sedimentary structures	Lithology	Component		Depositional environment	Water depth (m)
				Biotic	Abiotic		
Photozoan G/P (S16)	Centimeter to meter scale; blue, gray, tan	Planar tabular cross-stratification common, rare wave ripples	Local cauliflower chert nodules	Fusulinids, *Syringapora* coral heads, brachiopods, bryozoa, solitary corals, echinoderms, forams, trilobites	Common oolitic, oncolitic coatings, micritized sand-sized peloids; local cauliflower chert	Shoals and shorelines near to above FWWB	5–20 (a, e, g)
Thrombolite (S16b)	Decimeter-scale beds; blue	Micritic thrombolite, 1-5 cm diameter, <30 cm high, unknown synoptic relief; quartz and lime sand in troughs	Boundstone and grainstone	Abundant forams (commonly encrusting) common mollusks	Clotted micrite, coated grains, fully micritized grains, peloids	Shallow subtidal, photic, swept by currents	1–5 (j)
Metazoan framestone (S16c)	Massive; tan	Decimeter- to meter- diameter bioherms and biostromes	Framestone, variably dolomitized	Tabulate corals (*Syringapora*), Chaetetes, matrix similar to F8 and F9)	Peloids, coated grains, fully micritized grains	Shallow subtidal, above FWWB, bioherms may baffle mud	<1–15 (a)
Coated G/P (S16d)	Decimeter to meter scale; blue-gray to tan	Planar tabular to trough cross-stratified	Grainstone to packstone	Mostly as nuclei: fusulinids, coral fragments, brachiopods, bryozoa, echinoderms, forams, trilobites	Oncolitic to oolitic cortices; local cauliflower chert anhydrite pseudomorphs	Shallow, wave-washed shoals and shorelines, above FWWB	0–5 (a, d, g, h, i)
Lagoonal photozoan W/P (S17)	Decimeter to meter scale or massive; gray to tan	Typically thoroughly bioturbated, local grainy traction deposits	Wackestone and packstone, variable dolomite, chert nodules	Common whole brachiopod valves and shells, forams, fusulinids, bryozoa, solitary corals trilobites and articulated echinoderms; mollusk molds; rare chaetetes, sponges and Syringapora coral heads	Peloidal matrix, common oncolitic coatings, rare oolitic coatings, thick micrite envelopes	Evaporative lagoon	2–20 (a, e)
Dolomitized photozoan W/P (S17b)	Decimeter to meter scale or massive; tan	Typically thoroughly bioturbated, local grainy traction deposits	Dolowackestone and packstone, variably cherty	Common large fusulinids, brachiopods (spines), bryozoa, crinoids	Abundant peloids; common cauliflower chert pseudomorphs after anhydrite	Shallow, highly restricted, evaporative lagoon	2–5 (a, e)
Laminite (S18)	Centimeter to decimeter scale; tan, locally blue	Planar millimeter to centimeter laminations of mud and peloids/skeletal grains, mudcracks, crinkly with LLH stromatolites, cut and fill structures	Dolomudstone, wackestone, and packstone	Brachiopods (spines), trilobites; rare bryozoa, fusulinids	Peloids, coated grains; common cauliflower chert pseudomorphs after anhydrite	Intertidal to supratidal; crypt-microbial laminites	0–2 (k)
Dolomudstone (F19)	Massive; tan	Rare millimeter lamination	Dolomudstone with abundant cauliflower chert	Rare thin-walled brachiopods, abraded echinoderm fragments, bryozoa, and fusulinids	Peloids; common to abundant cauliflower chert after anhydrite; rare calcite pseudomorphs after swallowtail gypsum	Highly restricted lagoon	0–5 (a, e)
Paleosol (S20)	Centimeter to meter scale; yellow-red-brown	Roots, glaebules, circum-granular cracks, soil pisoids; ped structure, horizonation, slickensides	Calcisols, Protosols, Argilisols, and Vertisols	Those of overprinted limestone facies; rhizoliths and redoximorphic root haloes	Soil pisoids	Soil	0 (l)
Calcareous sandstone (S21)	Irregular centimeter scale		Silty, sandy palimpsest		Quartz silt to medium sand	Eolian, reworked during transgressions	0 (l)
Massive silty carbonate (S22)	Massive; reddish, yellowish tan	Locally millimeter laminated	Siltstone with carbonate cement/matrix	Few: phosphatic brachiopods, ostracodes; rare thin-walled brachiopods, abraded echinoderm ossicles, and solitary corals	Quartz silt and sand, mica flakes	Shallow estuarine	2–20

Note: G/P—pack-grainstone; W/P—wacke-packstone; LLH—laterally linked hemispherical; FWWB—fair weather wave base. (a) Above FWWB, (d) within photic zone, (e) Purser and Evans (1973), (g) Hagan and Logan (1974), (h) Loreau and Purser (1973), (i) Harris (1979), (j) Osleger and Read (1991), (k) intertidal, and (l) supratidal.

stromatolites, thrombolites, fusulinids, colonial corals, and dasyclad and other green algae, as well as most grains common to the heterozoan assemblage (e.g., James, 1997).

Outer-ramp lithofacies consist of mud- and calcisilt-rich heterozoan carbonates that were deposited largely below the influence of storm waves. Middle-ramp lithofacies consist of heterozoan and photozoan wacke-packstones that were deposited from storm wave base (SWB) to fair weather wave base (FWWB). Inner-ramp facies consist of pack-grainstone shoals and the variably restricted photozoan wacke-packstones, laminites, and restricted siliciclastic facies deposited in their lee. By late Pennsylvanian time, the Bird Spring platform had evolved into a shelf, and shelf interior facies were deposited in Arrow Canyon. These facies consist of more open photozoan pack-grainstones and more restricted, variably dolomitized wacke-packstones, evaporative dolomudstones, and laminites. They reflect deposition in shelf interiors that were episodically restricted, highly evaporative, and aggraded to sea level.

Outer-Ramp Facies

Outer-ramp lithofacies (Table 1) consist of fine-grained carbonates common in uppermost Chesterian to Desmoinesian (Serpukhovian to Moscovian) strata, and siliciclastic mudstones common in upper Chesterian (Serpukhovian) strata. Outer-ramp facies include marls (OR1), wavy interbedded cherts and calcisiltites (OR2), and massive to laminated calcisiltites (OR3) (Fig. 2). These fine-grained carbonates have a calcisiltite or mud matrix, common spicule

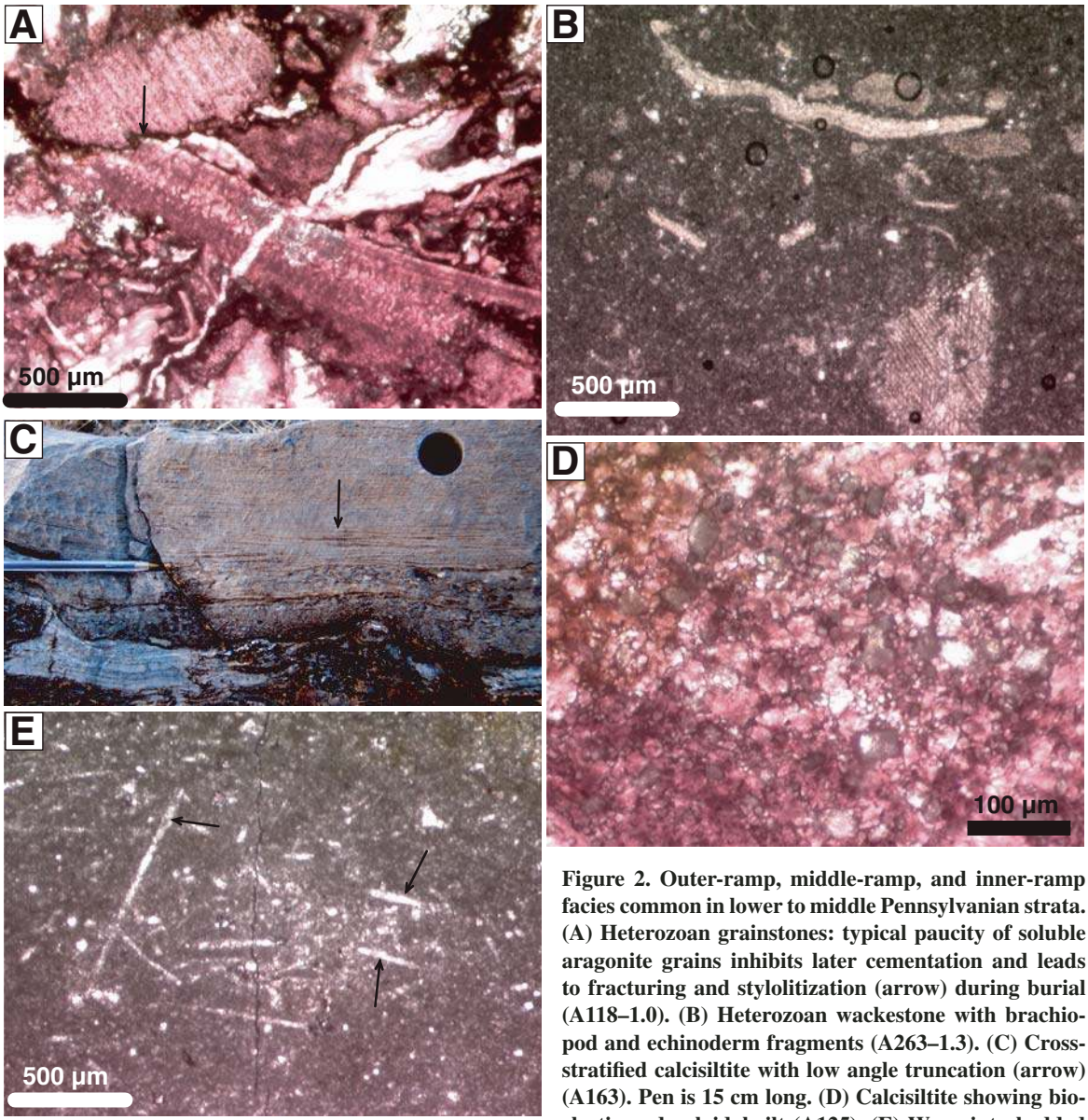

Figure 2. Outer-ramp, middle-ramp, and inner-ramp facies common in lower to middle Pennsylvanian strata. (A) Heterozoan grainstones: typical paucity of soluble aragonite grains inhibits later cementation and leads to fracturing and stylolitization (arrow) during burial (A118–1.0). (B) Heterozoan wackestone with brachiopod and echinoderm fragments (A263–1.3). (C) Cross-stratified calcisiltite with low angle truncation (arrow) (A163). Pen is 15 cm long. (D) Calcisiltite showing bioclastic and peloidal silt (A125). (E) Wavy interbedded calcisiltite and chert, showing common sponge spicule molds (arrows) in limestone, suggesting that chert beds were derived from spicule silica remobilized during early diagenesis (A293–0.4).

molds, and where identifiable a heterozoan assemblage of fossils.

Outer-ramp lithofacies were deposited below SWB, delineated by lime mud- and silt-sized particles, the absence of photozoan grain types, and an abundance of planar lamination. SWB in this interior seaway is estimated as between 30 and 60 m, based on modern analogs (e.g., Logan et al., 1969, 1970; Purser and Evans, 1973). An abundance of chert and spicule molds in these facies suggests that they formed in nutrient-rich waters, possibly associated with upwelling from the Keeler Basin (see following).

Outer-ramp siliciclastic lithofacies (Table 1) consist of millimeter- to centimeter-scale, laminated, quartz silt- and clay-rich mudstones, with rare marine fossils (IR4). Siliciclastic-rich deposits occur primarily in upper Chesterian strata and likely record regional siliciclastic influx derived from the Antler highlands to the west or the craton to the east (Poole and Sandberg, 1991; Trexler et al., 2004). The absence of cross-stratification suggests that these facies were deposited in quiet water, below FWWB and likely below SWB, possibly on a distal delta front (Bishop et al., 2009).

Middle-Ramp Facies

Middle-ramp lithofacies (Table 2) are divided into gently cross-stratified calcisiltites (MR5), heterozoan wacke-packstones (MR6), and photozoan wacke-packstones (MR7). These facies are abundant in Morrowan to Desmoinesian strata. Cross-stratified calcisiltites (MR5) have gentle truncation surfaces that locally approach hummocky cross-stratification. Heterozoan wacke-packstones (MR6) have a heterozoan assemblage of fossils and a calcisiltite and/or muddy matrix. Photozoan wacke-packstones (MR7) have photozoan grain types, a matrix composed of locally peloidal lime mud, and lack the evaporites and early dolomitization common to inner-ramp and shelf interior photozoan wacke-packstones.

Gently cross-stratified calcisiltites are interpreted to reflect deposition at or near SWB. Wacke-packstones are interpreted to have been deposited below FWWB (7–20 m, Logan et al., 1969, 1970; Purser and Evans, 1973; Gischler and Lomando, 2005), where mud was not winnowed by waves or currents, and above SWB (30–60 m; Logan et al., 1969; Purser and Seibold, 1973), where laminae of sand-sized grains were deposited but subsequently largely obscured by bioturbation. Photozoan lithofacies are also constrained by the depth of the photic zone, estimated to be ~30 m in this muddy interior seaway (cf. Purser and Seibold, 1973; Foster et al., 1997). All of these sediments were deposited in unrestricted waters, seaward of skeletal banks and coated grain shoals, as suggested by their normal marine flora and fauna, general lack of early dolomitization, absence of evaporite pseudomorphs, and the progressive shoaling of these muddy carbonates into grainy ones within generally regressive meter-scale packages (see following cycle discussion).

Inner-Ramp Facies

Inner-ramp facies consist of higher-energy facies (pack-grainstones, thrombolites, metazoan framestones, cross-bedded sandstones) deposited above FWWB, as well as the lagoonal restricted facies deposited in their lee (lagoonal wacke-packstones, tidal laminites, laminated siltstones). They are common throughout Osagean to Desmoinesian strata.

Higher-energy facies are subdivided into heterozoan, photozoan, and siliciclastic facies (Table 3). Heterozoan pack-grainstones (IR9) have a heterozoan assemblage of fossils, locally a calcisilt or muddy matrix, and are common in Osagean to Desmoinesian strata. High-energy photozoan facies consist of skeletal, oolitic and/or oncolitic and/or peloidal pack-grainstones (IR10), thrombolitic boundstones (IR10b), and metazoan framestones (IR10c). Metazoan framestones are typically surrounded by grainstones or less commonly wackestones, implying baffling of wave energy. Thrombolites are cut by channels filled with grainstones, suggesting energetic environments, likely proximal to sea level (e.g., Osleger and Read, 1991). High-energy inner-ramp siliciclastic lithofacies consist of planar tabular to trough cross-stratified sandstones (IR8) that form thin-bedded to massive units, up to 5 m thick, in the upper Chesterian.

Low-energy inner-ramp facies consist of lagoonal wacke-packstones, cryptmicrobial to thick-laminites (IR13), and various siliciclastic facies (IR15). Lagoonal wacke-packstones rarely have a heterozoan fauna (IR11) and more commonly a photozoan (IR12) one, which can be partially dolomitized (IR12b).

Peritidal facies consist of millimeter-scale cryptmicrobial laminites and millimeter- to centimeter-scale thick-laminites (IR13). Cryptmicrobial laminites consist of even to crinkly millimeter-scale laminae of variably peloidal dolomudstone, with sparse mudcracks and laterally linked hemispherical stromatolites. Thick-laminites consist of millimeter- to centimeter-scale graded laminations of peloids and lime mud with sparse mudcracks. Both cryptmicrobial and centimeter-scale thick-laminites are locally cut by decimeter-scale channels with coarse, intraclast-rich fill (cut-and-fill structures).

Inner-ramp siliciclastic lithofacies consist of irregular beds and lenses of variably calcareous, quartz sand and silt (IR15) that commonly occur above flooding surfaces and exposure horizons. The thickest, in Atokan strata (A220), is ~4 m thick, consists of planar to low-angle cross-laminated calcareous siltstone, and occurs between a caliche and an outer-platform sulfidic marl. An earliest Morrowan siliciclastic sandstone also occurs as an ~1-m-thick massive siltstone to very fine sandstone with root haloes developed in its upper surface (A57).

High-energy inner-ramp facies are interpreted as shoals, skeletal banks, patch reefs, and more rarely, grainy foreshore deposits. Photozoan and heterozoan pack-grainstones were deposited near and above FWWB (~7–20 m; Logan et al., 1969, 1970; Purser and Evans, 1973; Gischler and Lomando, 2005), as indicated by a common lack of carbonate mud and, in many photozoan facies, coated grains. These grainstone shoals, framestones, and boundstones typically formed breaks behind which low-energy inner-ramp facies accumulated. Heterozoan and photozoan wacke- packstones are interpreted as lagoonal deposits based on a diverse flora and fauna and their position between high-energy facies and peritidal facies in generally regressive meter-scale cycles (see following). Thick and cryptmicrobial laminites (F14) were deposited on lower and upper intertidal flats, respectively (e.g., Hardie and Shinn, 1986; Elrick and Read, 1991).

Siliciclastic lenses (IR15) are common at cycle bases and are interpreted as lowstand deposits reworked during transgressions in the platform interior. Their occurrence above subtidal flooding surfaces as well as exposure horizons, coupled with their sedimentary structures, suggests a variety of transport mechanisms (eolian, fluvial, shallow marine). Local pin-stripe lamination with subtle truncation in the thick lower Atokan example (A220) suggests the local preservation of primary eolian sedimentary structures. The concentration of siliciclastic sediments at cycle bases suggests, for lowstands and early transgressive phases, either a proximal source only available episodically, systematic changes in (eolian?) transport direction or strength, or less dilution due to a diminished carbonate factory. The early Morrowan massive siltstone to very fine sandstone (A57) is interpreted as an eolian deposit due to its uniform grain size and root haloes developed in its upper surface.

Shelf Interior Facies

In mid-Desmoinesian through early Virgilian time, shelf interior facies were deposited in

Arrow Canyon (Table 4). Shelf interior lithofacies consisted of variably coated photozoan pack-grainstones, thrombolites, and metazoan framestones (S16), undolomitized (S17) to dolomitized (S17b) photozoan wacke-packstones, dolomudstones (S19), cryptmicrobial to thick-laminites (S18), and various siliciclastic facies (S21, S22). These facies are generally similar to those of the older inner ramp, described above. Notable distinctions are generally more abundant synsedimentary dolomitization, especially muddy sediments, and evaporite pseudomorphs, particularly in massive (up to 15 m thick) outcrop exposures of homogeneous, peloidal, very poorly fossiliferous dolomudstone (S19), with common to abundant cauliflower- and popcorn-chert (Fig. 3B). Replacement dolomites consist of fine to very fine crystalline (15–60 µm), subhedral to euhedral turbid crystals with planar boundaries. Cauliflower- or popcorn-cherts are centimeter-scale nodules that consist of chert, quartz, blocky calcite, dolomite, and felted fabrics of silicified former anhydrite as well as encapsulated dolomite rhombs that predate compaction (Fig. 3B). Swallowtail pseudomorphs of blocky calcite after gypsum are also rarely present.

Siliciclastic facies occur as thin irregular beds and lenses, which occur at flooding surfaces (S21). In addition, in Desmoinesian strata (A380), a 12-m-thick calcareous sandstone occurs (the Tungsten Gap chert); it has local planar lamination and rare phosphatic brachiopods, and is used as a marker bed across the Arrow Canyon Range.

Grain-dominated shelf-interior lithofacies (S16) were deposited in shallow, high-energy settings on the shelf, where tidal or wave energy winnowed mud. Muddy shelf interior lithofacies (S17, S17b, S18, S19) were deposited in shallow, generally restricted waters, as suggested by a low-diversity, restricted fauna, large fusulinids, thin-walled brachiopods, peloidal muddy matrix, common evaporite pseudomorphs, and the succession of dolomitized muddy facies above high-diversity grainy limestones within regressive meter-scale cycles (see following). Thick packages of homogeneous dolomudstone (S19), lacking bedding surfaces and with common to abundant cauliflower chert (some with encapsulated aphanocrystalline to fine crystalline dolomite rhombs) indicate long-lived concurrent dolomitization and displacive anhydrite growth under unchanging depositional conditions. We interpret this facies to have been deposited in highly restricted shallow lagoons under an arid climate regime, where postdepositional dolomitization was driven by seepage from overlying lagoonal waters or reflux from adjacent sabkah environments (e.g., Sears and Lucia, 1980; Kendall and Skipwith, 1969; Montañez and Read, 1992a, 1992b; Montañez and Osleger, 1993, 1996; Lehmann et al., 1998, 2000).

Silty carbonate lenses (S21) preserved at cycle bases are interpreted as lowstand deposits

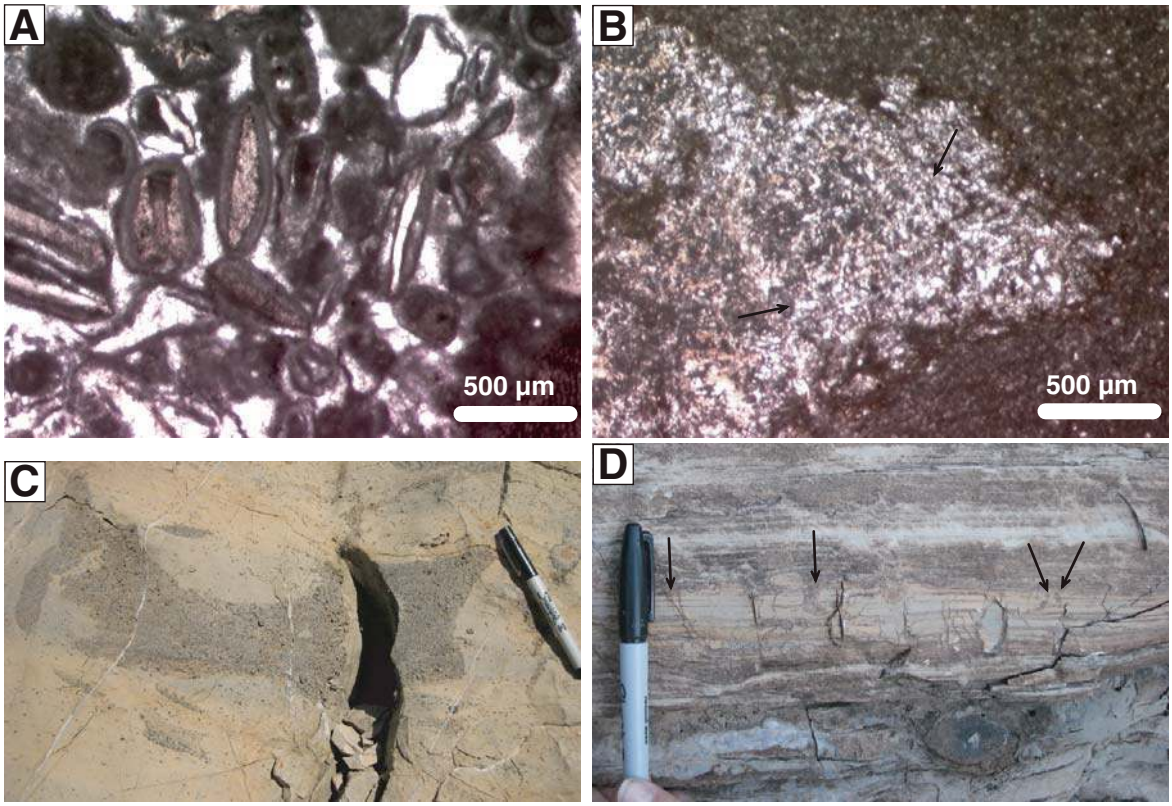

Figure 3. Upper Pennsylvanian shelf interior facies. (A) Oolitic grainstone with common moldic ooids and thin isopachous calcite cement (A445–1.2). (B) Peloidal dolomudstone disturbed by large, displacive popcorn-chert nodule. The nodule contains turbid rhombs of dolomite (gray) and silicified laths after anhydrite (white), lending it a felted fabric (arrows). The association of dolomite, anhydrite, and displaced lamination implies that anhydrite emplacement and dolomitization occurred concurrently during deposition and very shallow burial (A442–0.95). (C) Restricted dolomitic wackestone with cut-and-fill channel structure, filled with fusulinid tests (A475–0.5). Pen is 13 cm long. (D) Thick laminite with millimeter- to centimeter-scale lamination cut by desiccation cracks (arrows); ~11 cm of pen showing (A391–0.3).

reworked during ensuing transgressions. The thick Desmoinesian calcareous sandstone (Tungsten Gap Chert) likely formed in estuarine environments, on the basis of rare phosphatic brachiopods, the paucity of unabraded normal marine fossils, local flat lamination, and the absence of indicators for subaerial exposure.

Significant Surfaces

Significant surfaces are used to delineate meter-scale cycles. Five types of surfaces are observed in the Arrow Canyon succession, including flooding surfaces (1) and four types of subaerial exposure horizons: paleo-karst surfaces (2), meteorically altered surfaces (3), pedogenically altered surfaces (4), and deflation surfaces (5). Subaerial exposure horizons are common (n = 52) and are associated with extensive moldic porosity in the underlying limestones (though this feature is not considered unequivocally diagnostic of exposure; Melim et al., 2002). Subaerial exposure horizons are abundant in Chesterian and Morrowan (Serpukhovian and early Bashkirian) strata, common in Atokan and mid-Desmoinesian (upper Bashkirian and Moscovian) strata, and rare in upper Desmoinesian to lower Virgilian (Kasimovian and Gzhelian) strata. Flooding surfaces are common throughout Meramecian to Virgilian (upper Visean to Gzhelian) strata.

Flooding Surfaces

Flooding surfaces are recognized as abrupt contacts where more shoreward facies are retrogradationally overlain by more basinward facies. These surfaces can be sharp, erosive, or, more rarely, gradational. Facies above flooding surfaces are commonly enriched in insoluble material and locally have phosphatized grains. Flooding surfaces represent transgressions of the shoreline and mark cycle tops in the absence of subaerial exposure.

Karsted Horizons

Microkarst and macrokarst horizons are developed on subtidal limestones in lower Chesterian and mid-Desmoinesian strata. Microkarst surfaces are recognized as scalloped, pitted bedding planes with less than a few centimeters relief, whereas macrokarst is associated with centimeter- to decimeter-scale potholes, fissures, and dissolution pipes (Fig. 4). Karst surfaces are commonly filled by sandy palimpsest carbonate, terra rosa, sand- to cobble-sized lithorelicts, and/or millimeter- to meter-scale rhizoliths (e.g., Bishop et al., 2009). Roots, pebbles, and skeletal grains are commonly chertified and/or blackened with Fe and Mn oxides. Beneath karst surfaces, limestones have significant moldic porosity, which is commonly filled by Fe-poor (pink staining), nonluminescent meteoric cements. At a very well developed lower Chesterian karst horizon, several episodes of meteoric cementation and reworking occur; these have been interpreted to reflect missed sea-level beats and the landward merging of unconformities (Bishop et al., 2009).

Horizons of Meteoric Cementation

In Chesterian to Virgilian strata, meteoric cements fill primary and secondary porosity and are commonly associated with extensive moldic porosity; many of these surfaces do not exhibit karst or pedogenic features. Calcite cements are all nonferroan (stain pink with Dickson's solution) and nonluminescent to dully luminescent. They occur as micritic meniscus cements in primary pores (Fig. 4D), as very fine to fine crystalline equant calcites (crystal silt) that geopetally fill primary and secondary pores (commonly within rhizoliths; Fig. 4C), and as circumgranular isopachous cements with scalenohedral terminations and/or syntaxial overgrowths on echinoderm ossicles.

Meniscus cements and geopetal crystal silt are interpreted as vadose cements that formed during subaerial exposure (Dunham, 1969, 1971). Individual generations of vadose cements are not observed in successive cycles, suggesting that these cements are related directly to overlying cycle bounding surfaces. Nonferroan, nonluminescent circumgranular cements and syntaxial overgrowths on echinoderm ossicles are interpreted as phreatic cements that precipitated from oxidized meteoric waters (Bishop et al., 2009). Unless phreatic meteoric cements appear reworked, they are not considered diagnostic of subaerial exposure (i.e., they might have formed during subsequent unconformities). Vadose meteoric cements are considered diagnostic of subaerial exposure and can be the only indicator of exposure, or can be associated with karsted, rooted, and pedogenically altered horizons.

Deflation Surfaces

Four truncation surfaces are developed on highly restricted shelf interior dolomudstones in Missourian and Virgilian strata. These sharp surfaces exhibit as much as 20 cm of relief, place less restricted photozoan grainstone and/or wackepackstones over highly restricted dolomudstones, and are not associated with secondary porosity, meteoric cements, or karst features.

Truncation surfaces are interpreted as possible deflation surfaces that formed during sea-level falls when highly restricted, dolomitized, evaporite-rich sediments were exposed and deflated by winds, as noted on modern (Shinn, 1983; Hardie and Shinn, 1986) and ancient (Montañez and Read, 1992a, 1992b) arid tidal flats. The absence of an overlying lag, however, suggests that these horizons could also have formed by subaqueous erosion.

Pedogenically Altered Surfaces

Pedogenic features are abundant in upper Chesterian strata, common in Morrowan strata, and rare in Atokan, Desmoinesian, and Missourian strata. Pedogenic alteration occurs on both carbonate and siliciclastic substrates and ranges from rooted horizons indicative of ephemeral plant colonization to mature paleosol profiles.

Rooted horizons are typically developed on limestones and contain millimeter- to decimeter-scale roots that bifurcate downward. Roots are preserved as redoximorphic root haloes, carbonate and Fe-Mn oxide rhizoliths, and cherty compressions or adpressions. Root walls are commonly lined by carbonate and/or clay, and root casts are locally filled by meteoric cements (Fig. 4B). Rooted horizons commonly also contain grains and clasts blackened with Fe and Mn oxides.

Paleosols are distinguished and classified according to Mack et al. (1993) on the basis of their soil (ped) structure (fine granular to angular blocky, platy, rhomboid), horizonation, slickensides, extent of development of redoximorphic features, and evidence for translocation and accumulation of Fe and Mn oxides, phyllosilicates, carbonates, and organic matter. Chesterian paleosols in the Indian Springs and lowermost Bird Spring Formations include Argillisols, Calcisols, Vertisols, and Protosols (locally gleyed, ochric, or plinthitic), and were described at length in Bishop et al. (2009) (see also Richards et al., 2002; Barnett and Wright, 2008). Paleosol development in the overlying Pennsylvanian interval of the Arrow Canyon succession is limited to Calcisols (n = 3) and Protosols (n = 3).

Three paleosols occur in Atokan and Missourian strata and are characterized by $CaCO_3$ accumulation, occurring as irregular 1–20-cm-thick locally blackened crusts that veneer bedding planes. These crusts effervesce in H_2O_2, indicating a concentration of Fe and Mn oxides. They contain teardrop-shaped pisoids and laminations of silty carbonate (Fig. 4E). Carbonate rhizoliths are common and typically have geopetal fills of crystal silt. One of these paleosols crops out in lower Atokan strata as a white micritic bed, with local brown discoloration. In thin section, this horizon contains glaebules, defined by abundant circumgranular cracks and rhizoliths (Fig. 4F).

These paleosols are interpreted as Calcisols because their most prominent feature is the accumulation of pedogenic $CaCO_3$. Blackened

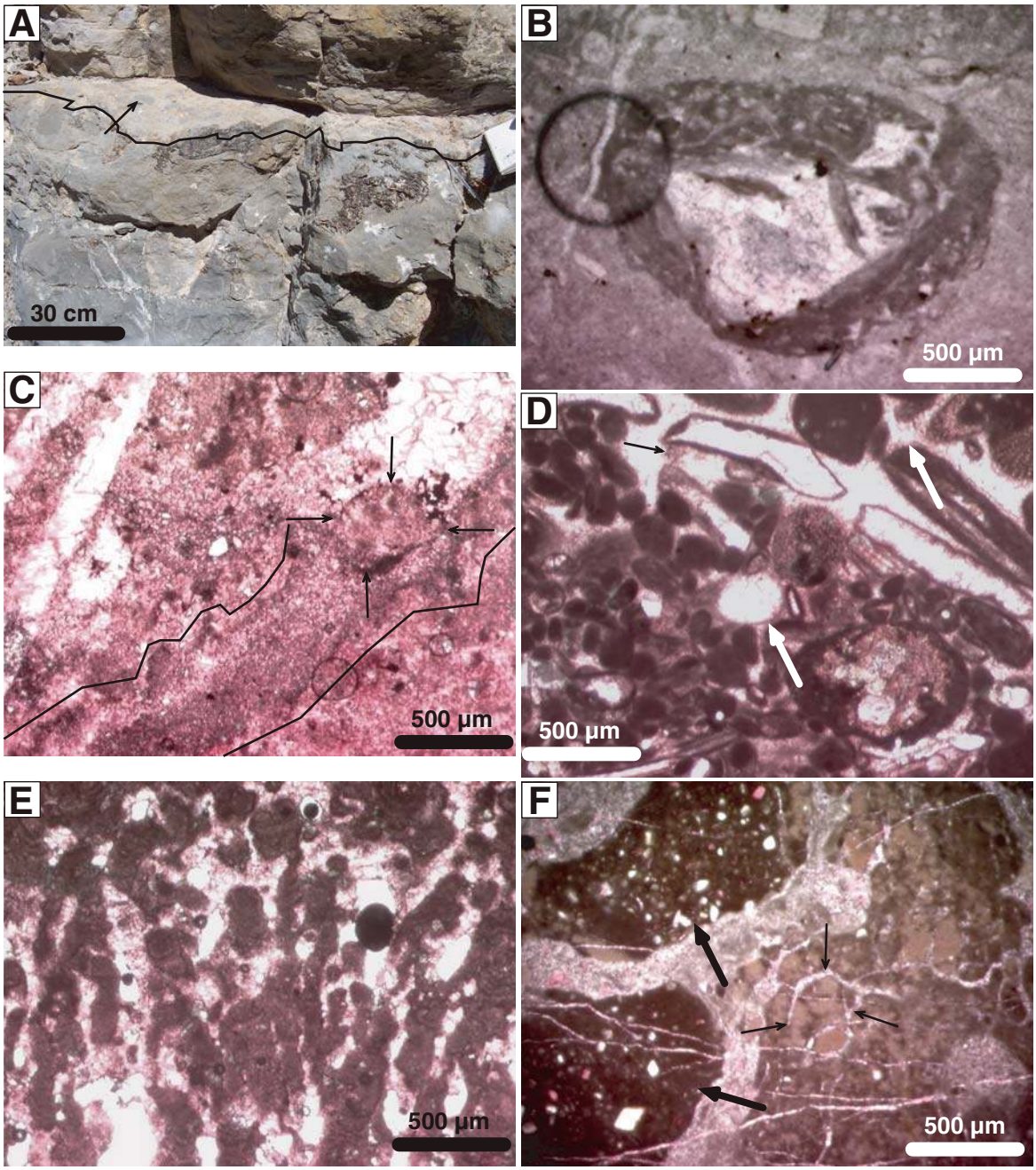

Figure 4. Subaerial exposure features. (A) Karst surface (black line), with fill of sandy palimpsest grains and lithorelicts (arrow) (A355–0.5). (B) Photomicrograph of rhizolith, with laminated peloidal carbonate coating (A-0). (C) Root cast (black outline) with geopetal fill of crystal silt and a displaced intraclast (arrows). Upper part of root cast occluded by blocky spar (A-0). (D) Peloidal grainstone with molds after aragonitic grains; vadose cementation indicated by bridging (black arrow) and meniscus (white arrows) micritic cements. Rare beach deposit at A83–0.5. (E) Stage 3-4 pisolitic calcrete (Machette, 1985). Teardrop-shaped pisoids are commonly microstalactitic (A460–1.2). (F) Calcrete with two generations of circumgranular cracks, defining dark brown (large arrows) and green-brown (small arrows) glaebules (A218–0.8).

crusts record vadose meteoric processes and are distinguished from modern outcrop patina by the teardrop-shaped pisoids, which are oriented perpendicular to bedding (rather than modern-day "down"). Although the accumulation of pedogenic carbonate on limestone parent material must be interpreted climatically with caution, these Calcisols likely reflect a subhumid to semiarid climate regime (Royer, 1999; Gong et al., 2005).

One interval of upper Morrowan strata contains three stacked, weakly developed brown to gray horizons with redoximorphic root haloes and platy ped structure; they pass downward into olive-brown wackestones with marine fossils. These are classified as Protosols due to weakly developed soil features. No climate interpretation can be made on the basis of these immature soil profiles.

METER-SCALE CYCLES

Facies are distributed stratigraphically into meter-scale progradational-retrogradational packages, bounded by disconformities or flooding surfaces. These packages are 15 cm to 19.5 m thick, averaging 3.5 m; they are referred to as cycles because each represents one cycle of retrogradation and progradation, despite not always exhibiting a predictable succession of facies (cf. Wilkinson et al., 1997, 1998). These cycles are classified according to their bounding surface and uppermost facies (i.e., disconformities developed on peritidal sediments, disconformities developed on subtidal sediments, and conformable flooding surfaces developed on subtidal sediments), and are further characterized by the dominant position of constituent facies on the platform (i.e., inner, middle, and outer ramp, or shelf interior). Representative facies belts and cycles for different intervals of time are shown in Figures 5–7. Figures 8–15 show representative windows of Arrow Canyon strata with outcrop photos and stratigraphic logs, and illustrate how facies and significant surfaces stack to form meter-scale cycles. (For a complete Arrow Canyon log, see Bishop, 2008.)

Peritidal Cycles

Peritidal cycles consist of subtidal lithofacies capped by intertidal facies with sharp to erosive bounding surfaces. Peritidal cycles are common in Meramecian and early Morrowan inner-ramp settings, and in late Desmoinesian to Virgilian shelf interior settings (Figs. 5–7, 9, and 15).

Peritidal cycles in Meramecian and lower Morrowan rocks were deposited in inner-ramp settings and consist of heterozoan (IR9) and photozoan (IR10) pack-grainstones that commonly pass upward into lagoonal wacke-packstones (IR11, IR12, IR12b) and are capped by tidal laminites (IR13) (Figs. 2D and 9). Generally, middle- to inner-platform peritidal cycles reflect shallowing from near FWWB to sea level.

In late Pennsylvanian strata, peritidal cycles are preserved in shelf interior settings and are capped by tidal laminites (S18), with cycle bases of lagoonal photozoan wacke-packstones (S17, S17b) that increase in restriction upward (increasing mud, dolomite, and evaporite pseudomorphs, and decreasing faunal diversity and abundance) (Figs. 7C and 15). Rarely, cycle bases consist of photozoan pack-grainstones (S16) that pass upward into restricted lagoonal facies (S17b) and tidal laminites (S18). These cycles reflect increasing restriction due to aggradation and/or progradation and the filling of accommodation, from above FWWB to sea level.

Disconformable Subtidal Cycles

Disconformable subtidal cycles contain exclusively subtidal facies and are bounded on their upper surface by a subaerial exposure horizon. These cycles occur throughout the Arrow Canyon succession, but are particularly abundant in Chesterian and Morrowan strata (e.g., Figs. 5–7).

In deposits that formed in outer-ramp settings, disconformable subtidal cycles contain marls (OR1) that pass upward into wavy interbedded chert and calcisiltite (OR2), massive to laminated calcisiltite (OR3), and cross-stratified calcisiltite (MR5), and are capped by subaerial exposure horizons. Exposure surfaces are commonly overlain by photozoan or heterozoan pack-grainstone transgressive deposits (IR9, IR10) (Fig. 6). Individual disconformable subtidal cycles commonly lack one or more of the lithofacies in these ideal cycles (Fig. 11). In upper Chesterian strata of the Indian Springs Formation, exposure-capped cycles consist of outer-ramp laminated siliciclastic mudstones (OR4) and inner-ramp heterozoan pack-grainstones (IR9); rooted horizons and paleosols may be developed on either of the constituent facies (Fig. 8). In Morrowan strata, very thin (<0.5 m) cycles consist of marls (OR1) overlain by heterozoan pack-grainstones (IR9) with rooting structures (Fig. 10). Outer-ramp exposure-capped cycles indicate shallowing from below SWB to above sea level (i.e., exposure).

In middle-ramp settings, disconformable subtidal cycles commonly contain either heterozoan (MR6) or photozoan (MR7) wacke-packstones that pass upward into pack-grainstones (IR9, IR10) and are capped by exposure horizons (Figs. 5 and 6). Disconformable subtidal cycles in middle-ramp settings reflect shallowing from below FWWB to above sea level.

In upper Pennsylvanian shelf interior settings, disconformable subtidal cycles are bounded by (possible) deflation surfaces, and in one instance a caliche. In these cycles, more open-marine photozoan pack-grainstones (S16) are overlain by muddy lagoonal facies (S17, S17b, S19) with stratigraphically upward increasing dolomite and evaporite pseudomorphs, and decreasing faunal diversity and abundance (Fig. 7). These facies transitions reflect increasing restriction across the shelf, culminating in truncation surfaces, which may represent deflation. In shelf interior settings, exposure-capped cycles reflect shallowing from above FWWB to above sea level.

Conformable Subtidal Cycles

Conformable subtidal cycles are bounded by flooding surfaces and are common throughout Meramecian to Virgilian strata in Arrow Canyon. Typically these cycles are composed of the same internal lithofacies as disconformable subtidal or peritidal cycles, but they lack subaerial exposure horizons and tidal flat facies.

In outer-ramp settings, conformable subtidal cycles contain marls (OR1) overlain by wavy interbedded chert and calcisiltite (OR2), massive to laminated calcisiltite (OR3), and cross-stratified calcisiltite (MR5). Cycle tops commonly contain a pack-grainstone deposit (IR9 or IR10; similar to the transgressive deposit in disconformable subtidal cycles) that likely formed during the sea-level lowstand or early transgression (Fig. 11). Such cycles reflect shallowing from below SWB to near FWWB. A few lower Desmoinesian cycles deepen upward and consist of basal photozoan grainstones (IR10) that pass upward into outer-ramp marls (OR1) and spiculitic calcisiltite (OR3), and are bounded at their tops by hardgrounds (i.e., omission surfaces) (A288–A296; Fig. 13). These are analogous to a combination of the give-up and catch-down cycles of Soreghan and Dickinson (1994), in that they reflect the temporary drowning of the ramp before relative sea-level fall brings the seafloor back within the zone of maximum production, resuscitating the carbonate factory.

In middle- to inner-ramp settings, subtidal cycles contain heterozoan (MR6) or photozoan (MR7) wack-packstones that coarsen upward into pack-grainstones (IR9, IR10; Figs. 10 and 14). These cycles also locally contain thin outer-ramp facies at their cycle bases (Fig. 12). In middle-ramp settings, conformable subtidal

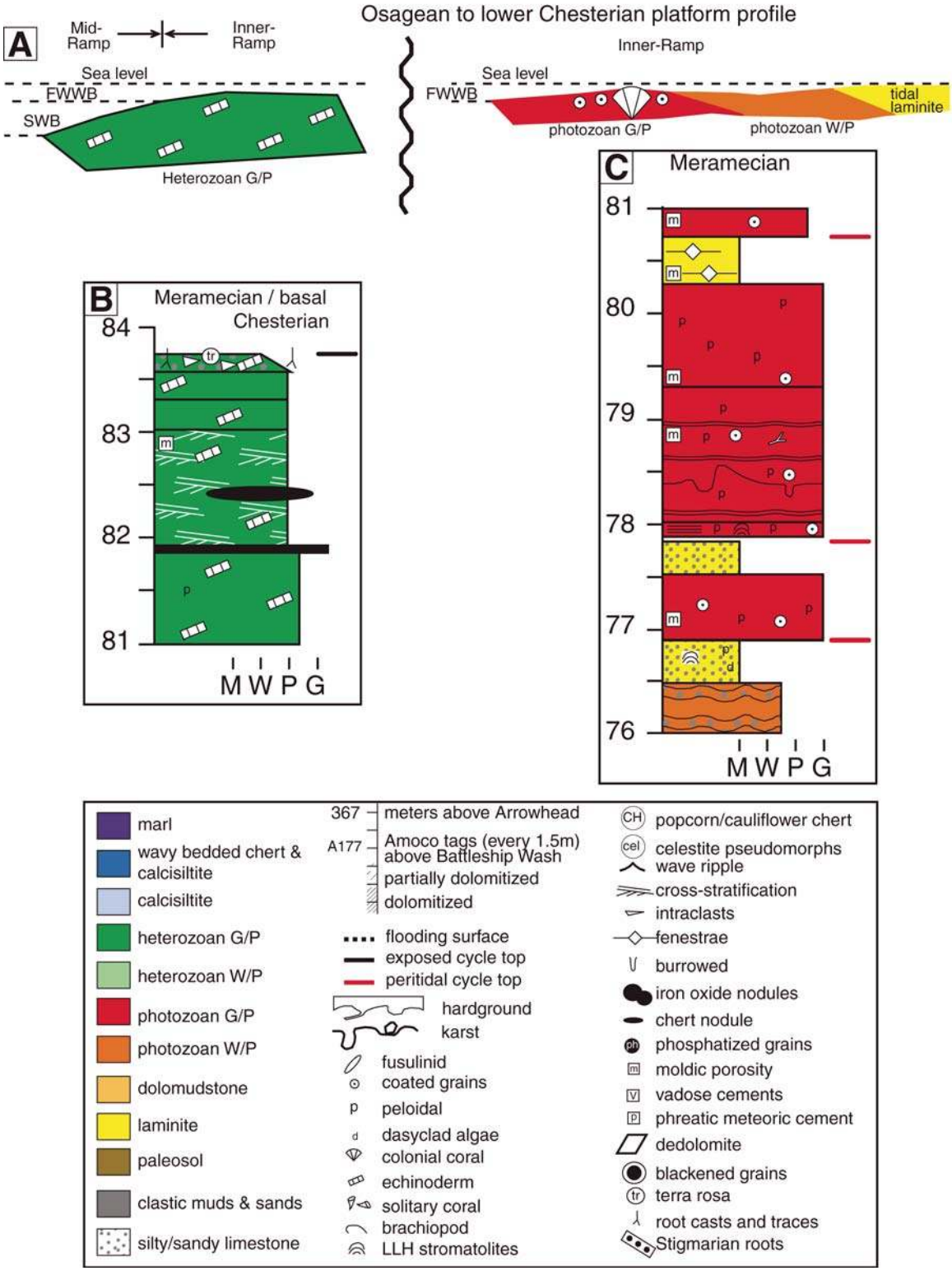

Figure 5. (A) Osagean to lower Chesterian depositional profile. Encrinite shoals (left) were likely coeval with more shoreward shallow photozoan sediments (right). G/P—pack-grainstone; W/P—wacke-packstone; FWWB—fair weather wave base; SWB—storm wave base. (B) Encrinites near the Meramecian-Chesterian boundary (late Visean), showing the initial subaerial exposure horizon marking the onset of glacioeustasy (Bishop et al., 2009). (C) Shallow, photozoan sediments of Meramecian age, with tidal flat facies and peloidal, locally oncolitic pack-grainstones. In key, LLH is laterally linked hemispherical. Scale in meters above the top of the Arrowhead Formation.

cycles reflect changes in relative sea level from near SWB to near to above FWWB.

In shelf interior settings, conformable subtidal cycles have photozoan lime pack-grainstones (S16) at their bases, passing upward into increasingly restricted, dolomitized lagoonal photozoan wack-packstones (S17, S17b, S19; Fig. 15). These cycles are bounded by flooding surfaces and contain facies that increase in their degree of restriction upward, yet did not shallow completely to intertidal depths.

Noncyclic Interval

Osagean (lower Visean) strata in the Yellowpine Formation contain a noncyclic interval consisting of ~60 m of massive, poorly bedded echinoderm pack-grainstones (IR9). These carbonates are consistent with deposition adjacent to stable echinoderm banks, which were common during Mississippian time (Kammer and Ausich, 2006). This interval contains no facies changes or exposure horizons, suggesting continuous deposition between SWB and FWWB (Bishop et al., 2009).

CARBONIFEROUS STRATIGRAPHIC AND CLIMATIC RECORD

Long-term Accommodation History

Long-term sedimentary accumulation rates for Arrow Canyon demonstrate that local variations in accommodation from middle

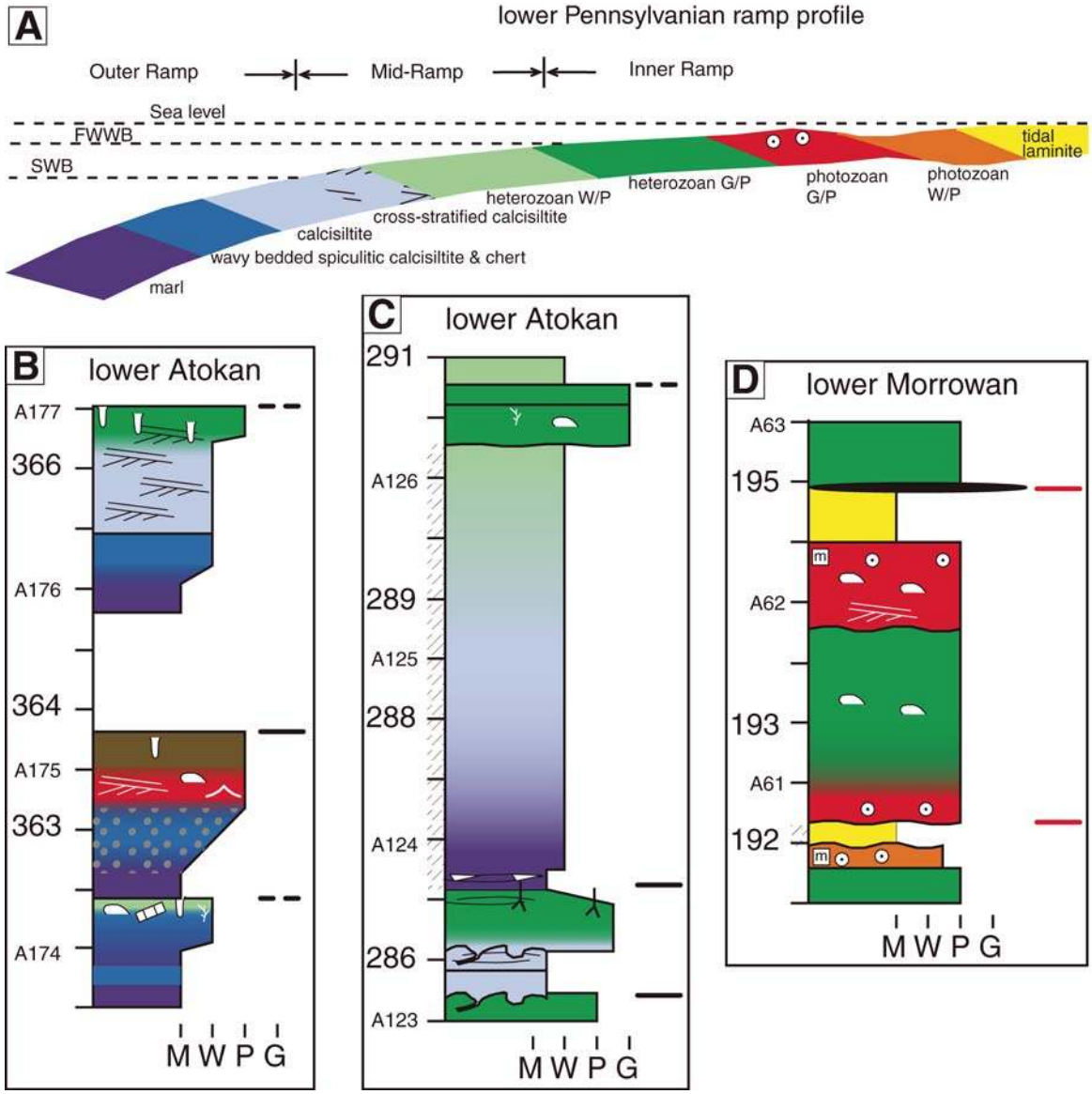

Figure 6. Lower Pennsylvanian deposition. (A) Schematic showing profile of distally steepened Bird Spring ramp with distribution of contemporaneous facies (see Tables 1–3). (B) Lower Atokan cycles with regressive outer-ramp facies successions and thin middle- to inner-ramp packstones, locally exposure capped. (C) Lower Atokan cycles with outer-platform bases and inner-ramp to subaerially exposed cycle tops. (D) Lower Morrowan mixed heterozoan-photozoan cycles capped by thick laminites with sharp to erosive bounding surfaces. Scale in both meters above the top of the Arrowhead Formation (large numbers) and Amoco numbers (A = 1.5 m) measured from the top of the Battleship Wash Formation. See Figure 5 for legend.

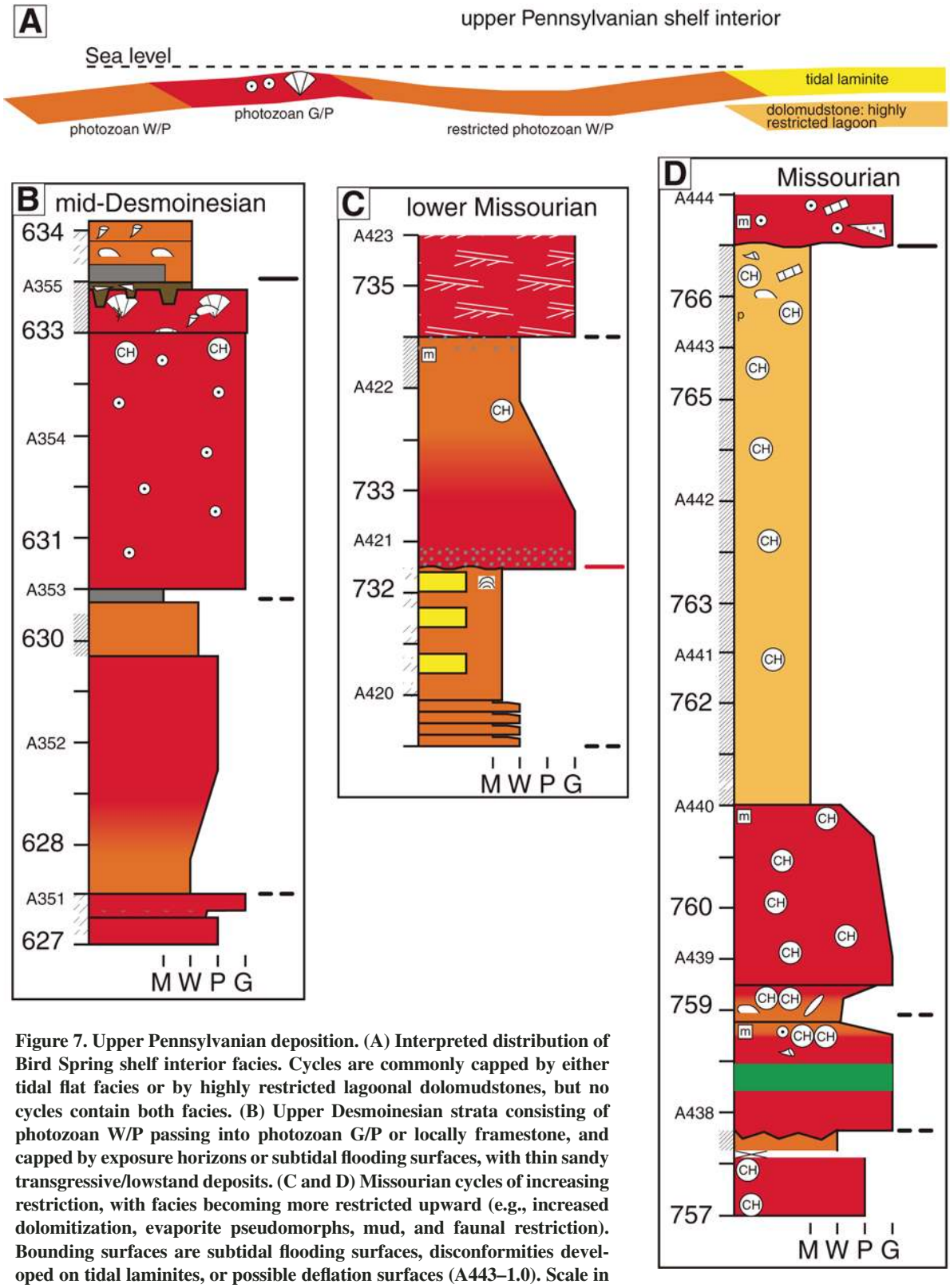

Figure 7. Upper Pennsylvanian deposition. (A) Interpreted distribution of Bird Spring shelf interior facies. Cycles are commonly capped by either tidal flat facies or by highly restricted lagoonal dolomudstones, but no cycles contain both facies. (B) Upper Desmoinesian strata consisting of photozoan W/P passing into photozoan G/P or locally framestone, and capped by exposure horizons or subtidal flooding surfaces, with thin sandy transgressive/lowstand deposits. (C and D) Missourian cycles of increasing restriction, with facies becoming more restricted upward (e.g., increased dolomitization, evaporite pseudomorphs, mud, and faunal restriction). Bounding surfaces are subtidal flooding surfaces, disconformities developed on tidal laminites, or possible deflation surfaces (A443–1.0). Scale in both meters above the top of the Arrowhead Formation (large numbers) and Amoco numbers (A = 1.5 m) measured from the top of the Battleship Wash Formation. See Figure 5 for legend and abbreviations.

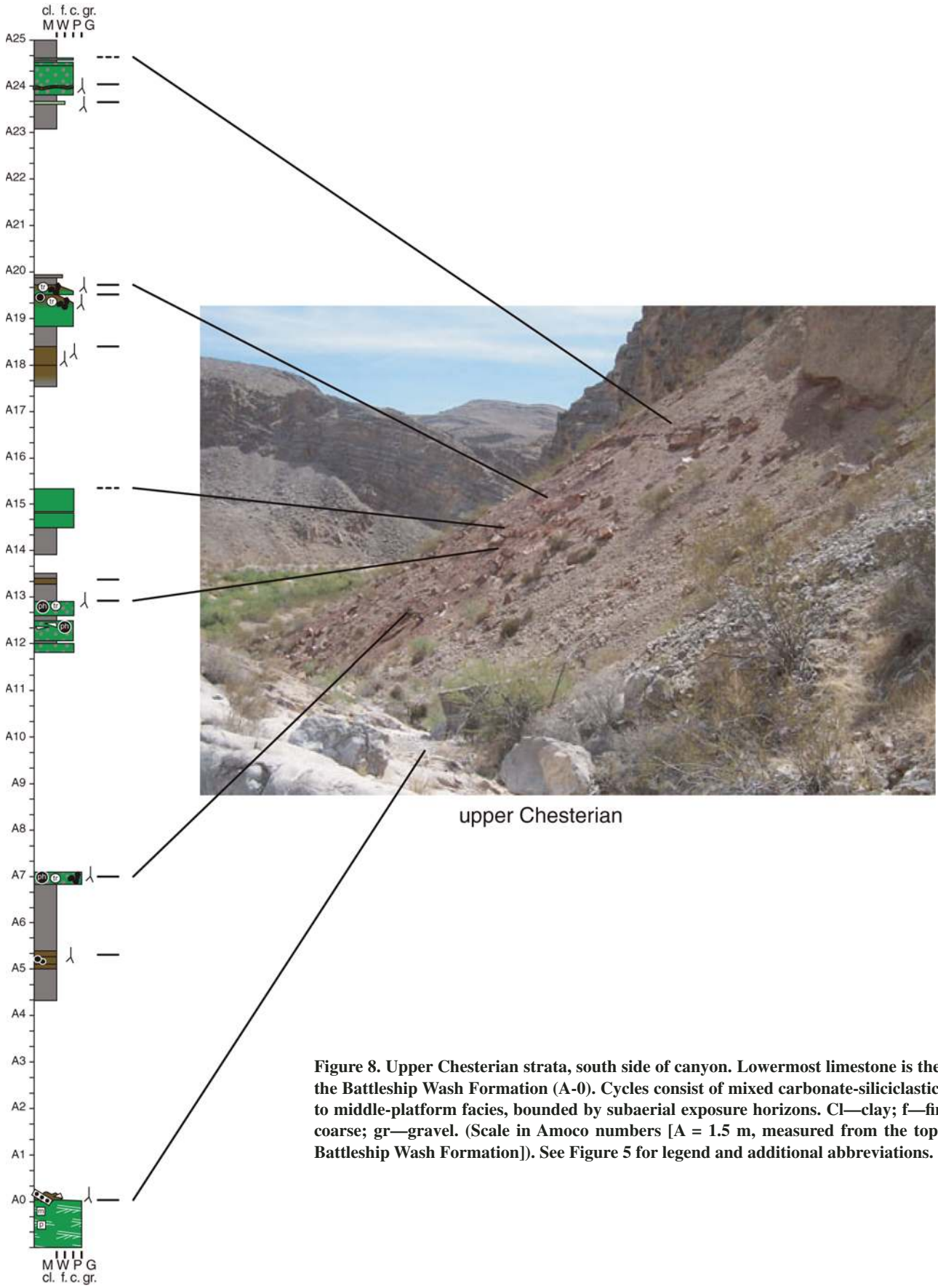

Figure 8. Upper Chesterian strata, south side of canyon. Lowermost limestone is the top of the Battleship Wash Formation (A-0). Cycles consist of mixed carbonate-siliciclastic outer- to middle-platform facies, bounded by subaerial exposure horizons. Cl—clay; f—fine; c—coarse; gr—gravel. (Scale in Amoco numbers [A = 1.5 m, measured from the top of the Battleship Wash Formation]). See Figure 5 for legend and additional abbreviations.

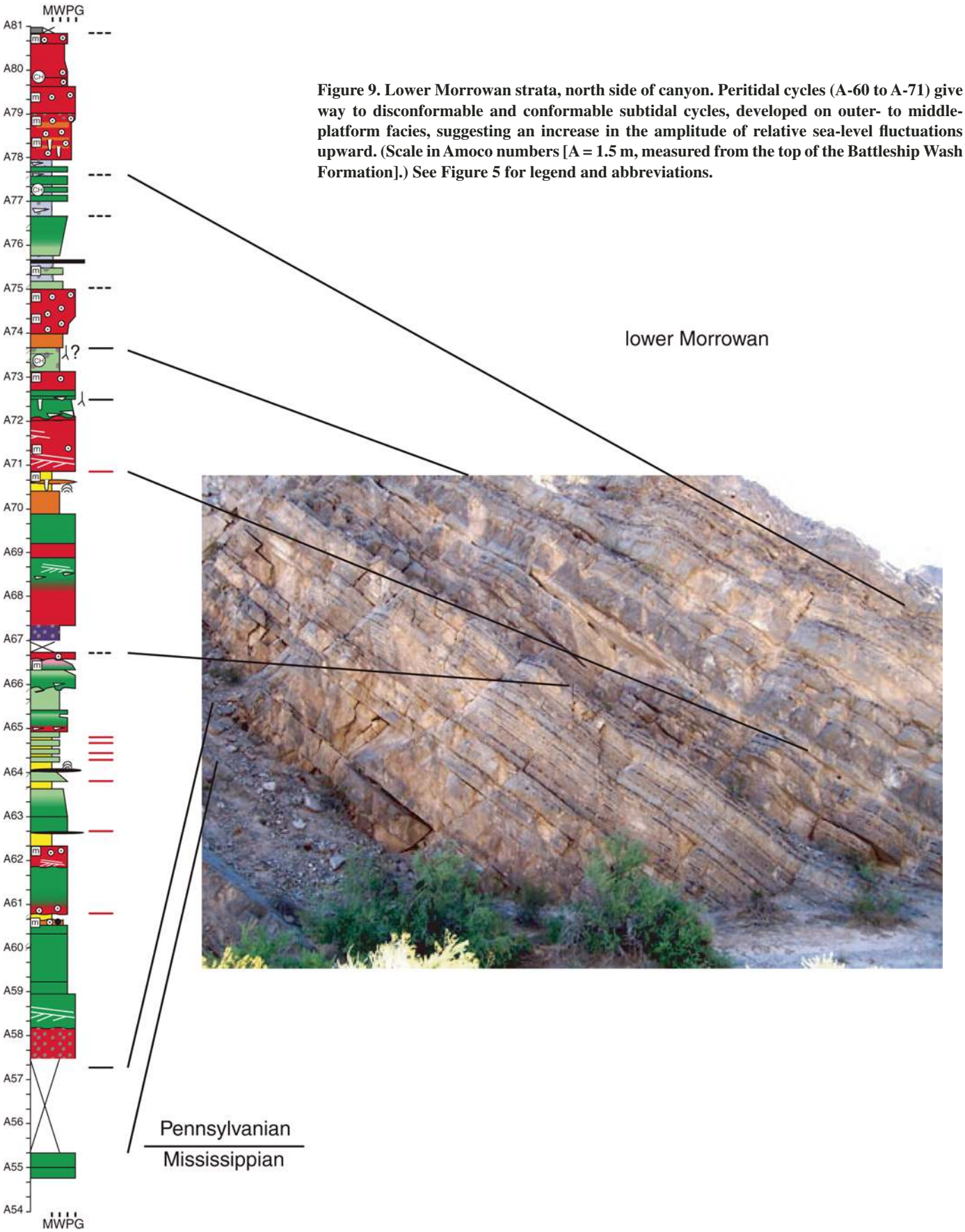

Figure 9. Lower Morrowan strata, north side of canyon. Peritidal cycles (A-60 to A-71) give way to disconformable and conformable subtidal cycles, developed on outer- to middle-platform facies, suggesting an increase in the amplitude of relative sea-level fluctuations upward. (Scale in Amoco numbers [A = 1.5 m, measured from the top of the Battleship Wash Formation].) See Figure 5 for legend and abbreviations.

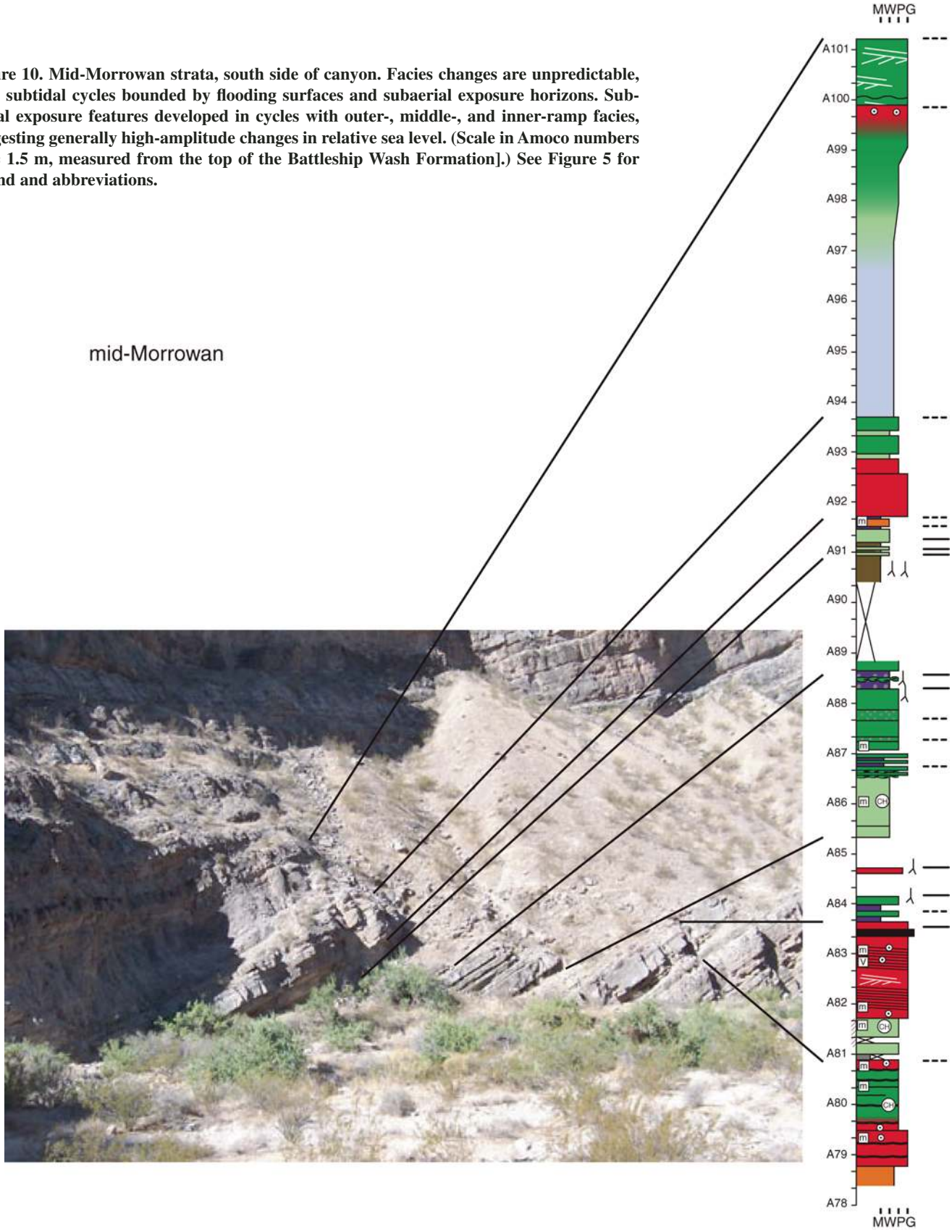

Figure 10. Mid-Morrowan strata, south side of canyon. Facies changes are unpredictable, with subtidal cycles bounded by flooding surfaces and subaerial exposure horizons. Subaerial exposure features developed in cycles with outer-, middle-, and inner-ramp facies, suggesting generally high-amplitude changes in relative sea level. (Scale in Amoco numbers [A = 1.5 m, measured from the top of the Battleship Wash Formation].) See Figure 5 for legend and abbreviations.

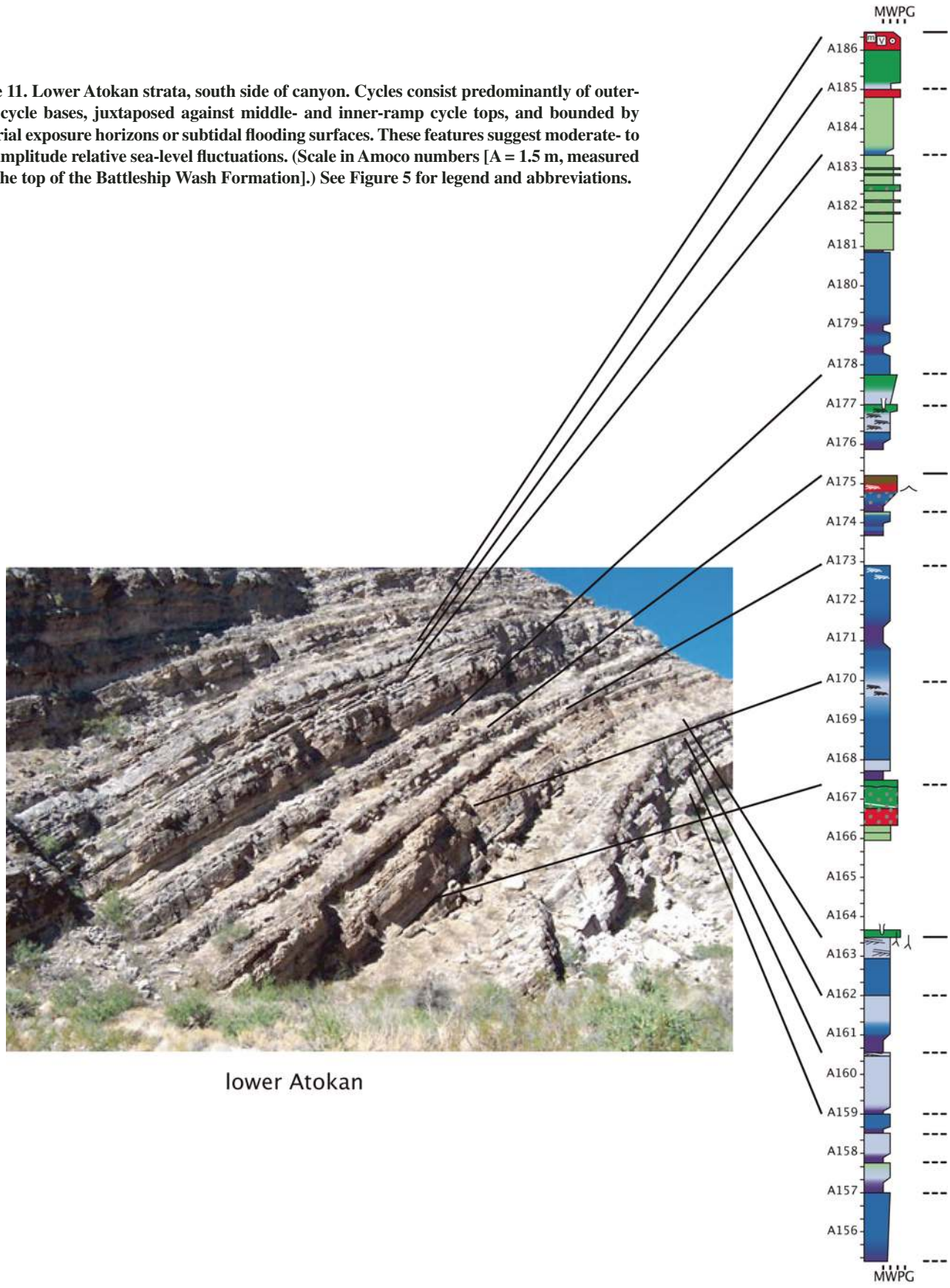

Figure 11. Lower Atokan strata, south side of canyon. Cycles consist predominantly of outer-ramp cycle bases, juxtaposed against middle- and inner-ramp cycle tops, and bounded by subaerial exposure horizons or subtidal flooding surfaces. These features suggest moderate- to high-amplitude relative sea-level fluctuations. (Scale in Amoco numbers [A = 1.5 m, measured from the top of the Battleship Wash Formation].) See Figure 5 for legend and abbreviations.

Mississippian to end-Pennsylvanian time overwhelmed the global eustatic signal in this depositional setting. However, this locally controlled long-term accommodation trend provides a context in which to assess the nature of short-term relative sea-level fluctuations. Long-term accumulation rates were calculated based on rock thickness per stage, constrained by the integrated biostratigraphic zonation (Appendix A) and calibrated to the Gradstein et al. (2004) time scale. Most cycles shoal above SWB, so changes in this long-term accumulation plot primarily reflect changes in the creation of accommodation space, rather than how efficiently it was filled (Fig. 16C).

Figure 16C presents two accumulation plots for Arrow Canyon, determined using the North American and Russian Platform (global) stages, respectively. The differences in accumulation rates derive from the fact that, although in Arrow Canyon the North American stages are well constrained biostratigraphically, these stage boundaries are relatively poorly dated, relying on biostratigraphic correlations to better-dated Eurasian sections (e.g., Gradstein et al., 2004). In contrast, though global stages are more precisely dated, they are only loosely defined in Arrow Canyon, and North America in general. Thus, both age models have considerable uncertainty. However, despite the two plots differing in detail, they clearly document a similar long-term history of variations in accommodation space in the study area during the Carboniferous.

Estimated long-term sediment accumulation rates (Fig. 16C) indicate that accommodation

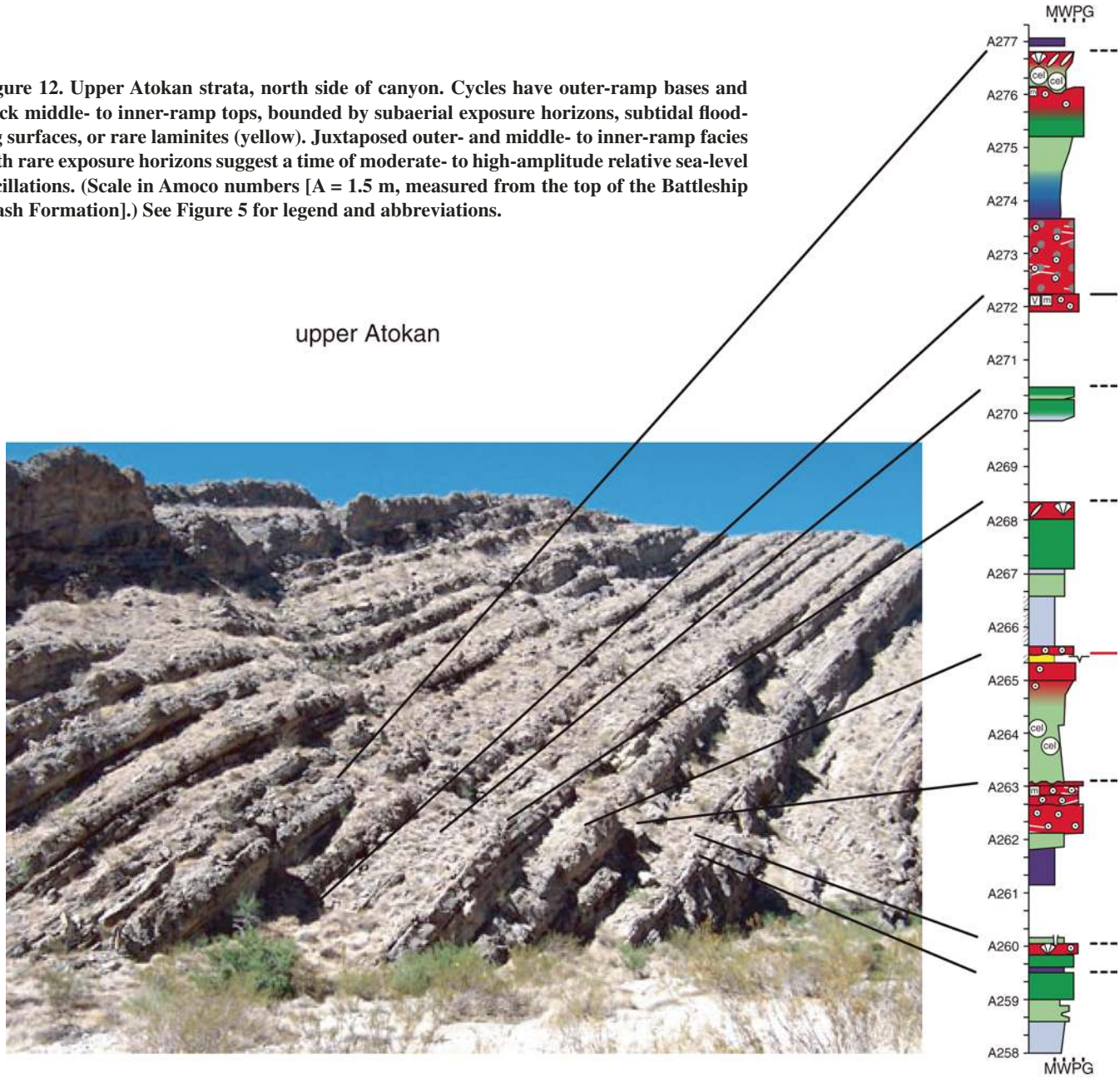

Figure 12. Upper Atokan strata, north side of canyon. Cycles have outer-ramp bases and thick middle- to inner-ramp tops, bounded by subaerial exposure horizons, subtidal flooding surfaces, or rare laminites (yellow). Juxtaposed outer- and middle- to inner-ramp facies with rare exposure horizons suggest a time of moderate- to high-amplitude relative sea-level oscillations. (Scale in Amoco numbers [A = 1.5 m, measured from the top of the Battleship Wash Formation].) See Figure 5 for legend and abbreviations.

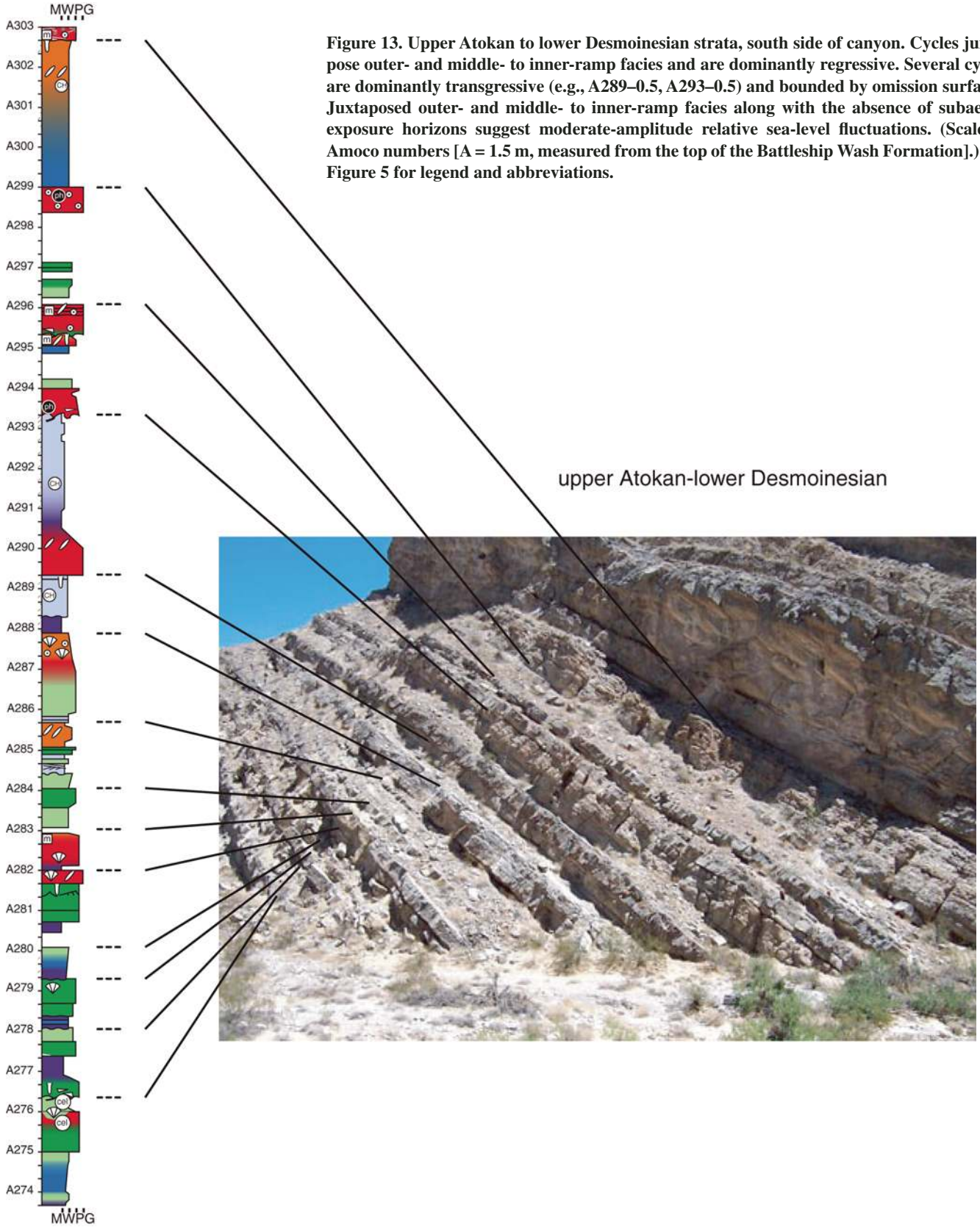

Figure 13. Upper Atokan to lower Desmoinesian strata, south side of canyon. Cycles juxtapose outer- and middle- to inner-ramp facies and are dominantly regressive. Several cycles are dominantly transgressive (e.g., A289–0.5, A293–0.5) and bounded by omission surfaces. Juxtaposed outer- and middle- to inner-ramp facies along with the absence of subaerial exposure horizons suggest moderate-amplitude relative sea-level fluctuations. (Scale in Amoco numbers [A = 1.5 m, measured from the top of the Battleship Wash Formation].) See Figure 5 for legend and abbreviations.

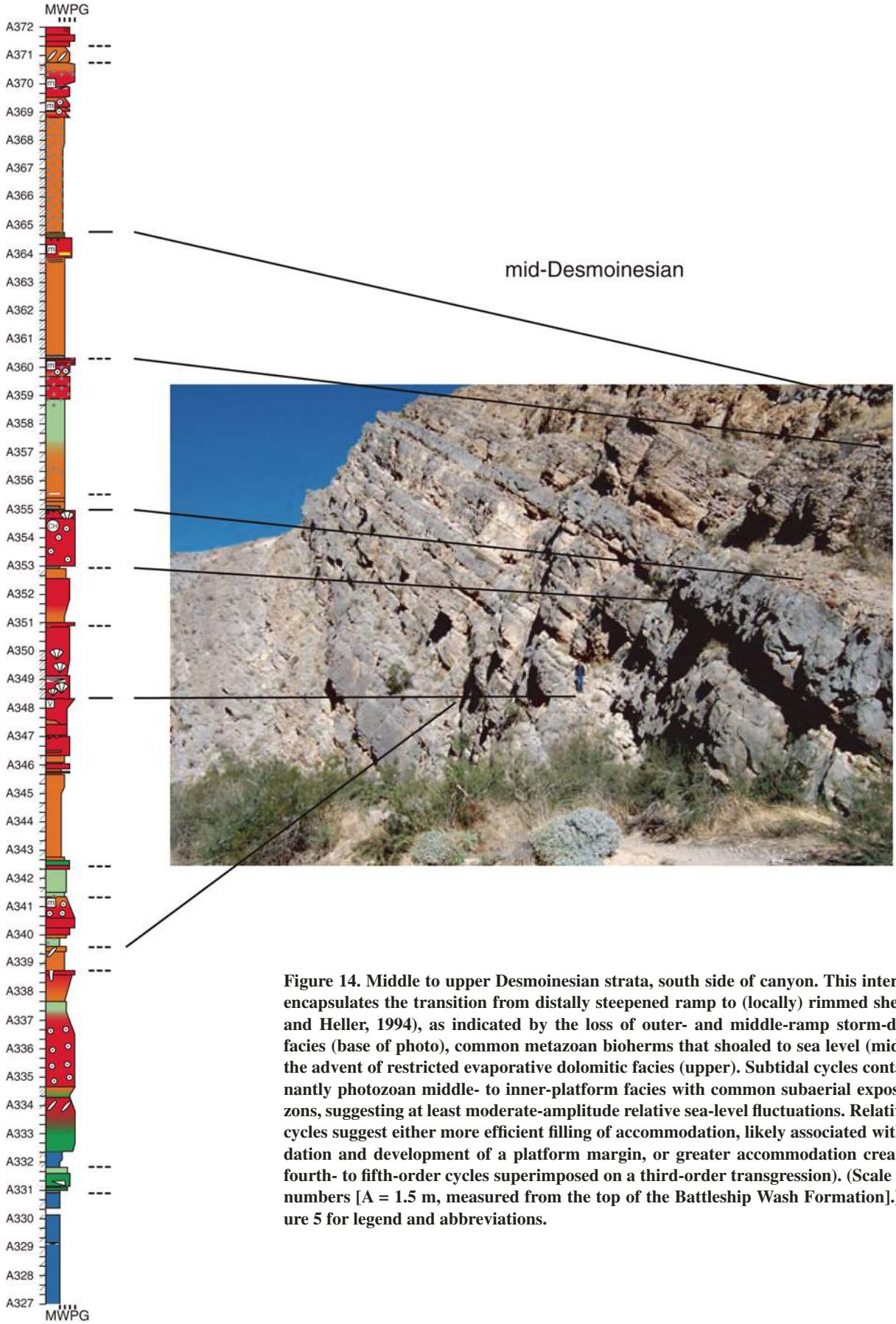

Figure 14. Middle to upper Desmoinesian strata, south side of canyon. This interval likely encapsulates the transition from distally steepened ramp to (locally) rimmed shelf (Miller and Heller, 1994), as indicated by the loss of outer- and middle-ramp storm-dominated facies (base of photo), common metazoan bioherms that shoaled to sea level (middle), and the advent of restricted evaporative dolomitic facies (upper). Subtidal cycles contain dominantly photozoan middle- to inner-platform facies with common subaerial exposure horizons, suggesting at least moderate-amplitude relative sea-level fluctuations. Relatively thick cycles suggest either more efficient filling of accommodation, likely associated with progradation and development of a platform margin, or greater accommodation creation (e.g., fourth- to fifth-order cycles superimposed on a third-order transgression). (Scale in Amoco numbers [A = 1.5 m, measured from the top of the Battleship Wash Formation].) See Figure 5 for legend and abbreviations.

was twofold to tenfold higher during the Morrowan through Missourian (20–70 m/m.y.) than during the Chesterian (7 m/m.y.) or Virgilian (12.6 m/m.y.), with greatest accommodation during the Atokan (68 m/m.y.) and Desmoinesian (59 m/m.y.). This long-term accommodation history likely reflects the combined effects of changes in tectonically driven subsidence in the Keeler Basin and second- and third-order (>1 m.y.) eustatic fluctuations. Notably, the Atokan maximum in accommodation occurs during a eustatic second-order regression and/or lowstand (Ross and Ross, 1987; Galonka and Kiessling, 2002). This suggests that long-term eustatic changes in this region were largely superseded by local subsidence. It is this local increase in subsidence that allows for the preservation of mostly complete high-amplitude, high-frequency cycles during the global sea-level lowstand. Similarly, during the late Pennsylvanian, diminished subsidence sensitizes the Arrow Canyon record to even moderate amplitude high-frequency changes in relative sea level, which should cause exposure of the shallow subtidal facies. Thus, the Arrow Canyon section provides a window of opportunity for capturing the full range of amplitudes of relative sea-level change when the creation of accommodation space is high (early to mid-Pennsylvanian), and constrains the maximum

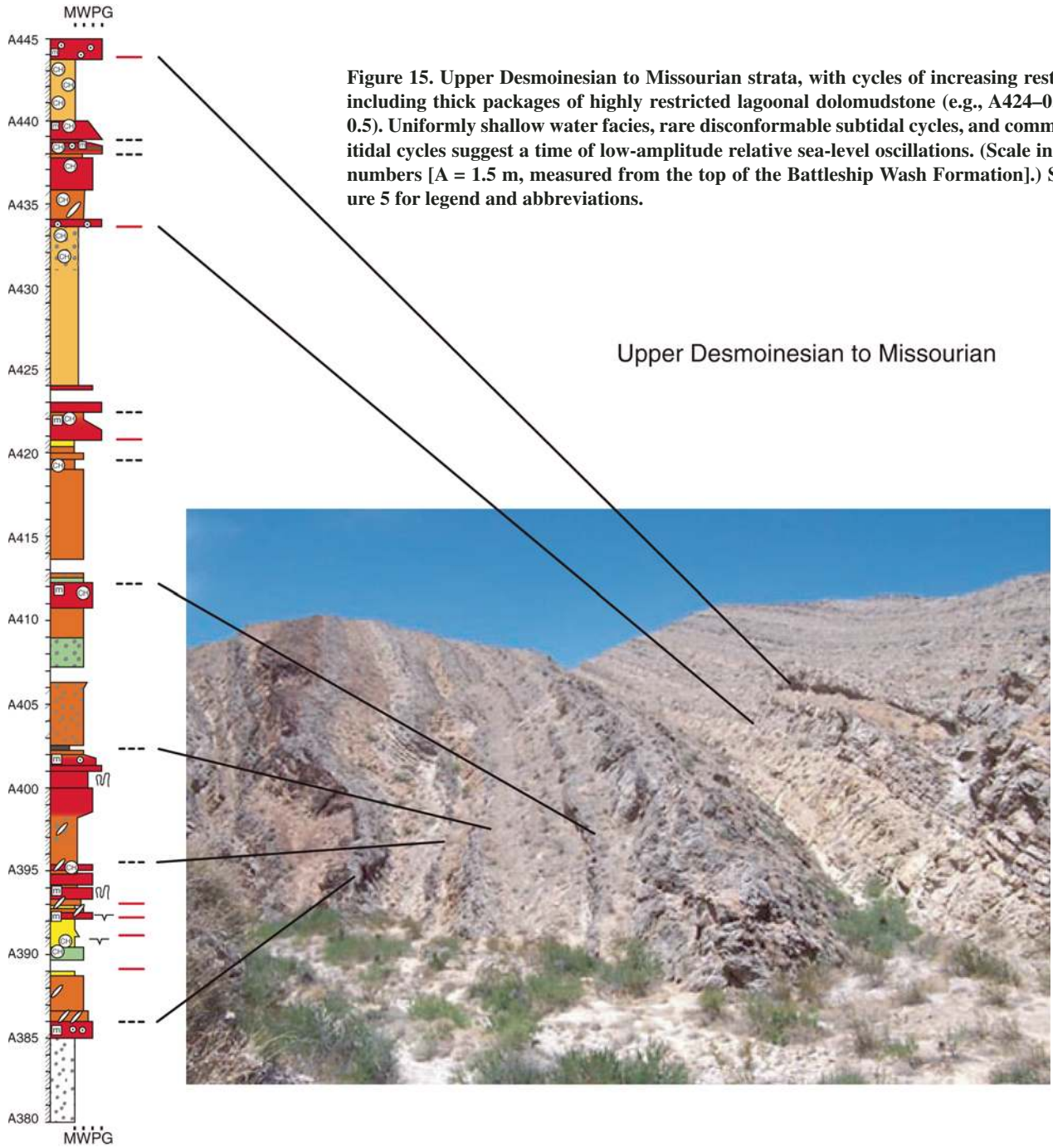

Figure 15. Upper Desmoinesian to Missourian strata, with cycles of increasing restriction, including thick packages of highly restricted lagoonal dolomudstone (e.g., A424–0.5–433–0.5). Uniformly shallow water facies, rare disconformable subtidal cycles, and common peritidal cycles suggest a time of low-amplitude relative sea-level oscillations. (Scale in Amoco numbers [A = 1.5 m, measured from the top of the Battleship Wash Formation].) See Figure 5 for legend and abbreviations.

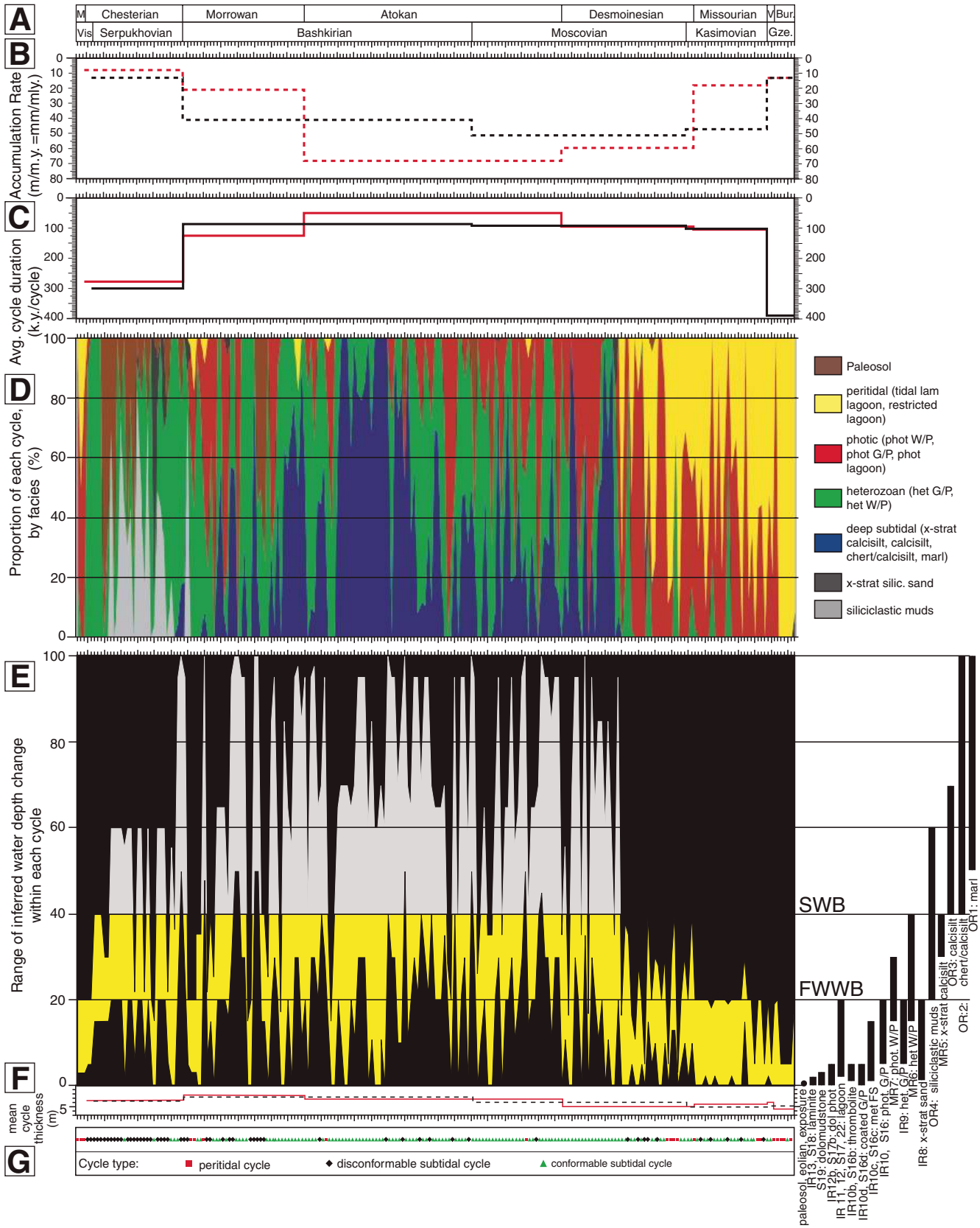

Figure 16. Relative sea-level history for Arrow Canyon, according to cycle number. (A) Carboniferous geologic stages, fitted to cycle number using all available biostratigraphy (Appendix A). (B) Long-term accumulation curve, as a proxy for accommodation. Rates estimated using North American (red) and global (black) stage boundaries. (C) Average cycle period according to stage, using North American (red) and global (black) stage boundaries. (D) Proportion of cycle made up of each facies association. Upper Mississippian to middle Pennsylvanian cycles have prominent outer-ramp facies; Upper Pennsylvanian cycles are dominated by shallow, restricted, and peritidal facies. (E) Range of relative sea-level change for each cycle, based on range of water depths inferred for the deepest and shallowest water facies present in each cycle. Colored areas represent band of possible amplitudes, with highest confidence in estimates less than the depth to storm wave base (SWB) (shown in yellow). The range of estimates represents a minimum for cycles with facies deposited below SWB or with disconformable bounding surfaces (e.g., Chesterian-Desmoinesian). Estimated ranges bracket the maximum magnitude for peritidal or conformable subtidal cycles with facies deposited above SWB (e.g., much of late Pennsylvanian). See text for further explanation. FWWB—Fair weather wave base. (F) Long-term average cycle thickness, as a proxy of subsidence per cycle. A more accurate estimate of eustatic amplitudes would subtract this thickness from the range in water depths inferred from constituent facies. (G) Distribution of cycle types. Intervals of low-amplitude relative sea-level changes (in the Meramecian, lower Morrowan, and upper Desmoinesian to Virgilian) are accompanied by more common peritidal cycles. See Figure 5 for abbreviations.

that sea level could have changed when accommodation creation was lowered (late Pennsylvanian), given that at such times accumulating carbonates would be very sensitive to any high-amplitude relative sea-level changes (i.e., tidal flats would be stranded landward and syndepositional dolomite would be limited; Read et al., 1986; Montañez and Read, 1992a).

Relative Sea-Level History

The history of short-term relative sea-level fluctuations is reconstructed using water depths inferred from the lithofacies in each cycle and the distribution of subaerial exposure horizons (Fig. 16). Ranges of water depths for each facies are calibrated to inferred depths for FWWB, SWB, and the photic zone based on sedimentary structures, grain types, and using modern and ancient facies analogs (Tables 1–4, and references therein). Comparisons between the deepest and shallowest facies in each cycle provide an estimated range of relative sea-level change within that cycle. These depth ranges are highly sensitive to inferred SWB and FWWB, which can vary significantly depending on geographic setting. For this Carboniferous shallow interior seaway, SWB is inferred to be 40 m and FWWB to be ~20 m, although FWWB can be considerably shallower (~8 m in the Persian Gulf; Purser and Evans, 1973; Gischler and Lomando, 2005) and SWB considerably deeper (~60 m in the Yucatan; Logan et al., 1969) on modern carbonate platforms. These values provide a relatively conservative estimate of sea-level changes. Amplitudes of sea-level change estimated beyond these wave-base thresholds are less well constrained; the maximum water depth for deep subtidal sediments is arbitrarily defined as 100 m but could have been greater. Overall, the magnitudes of sea-level falls may be underestimated where cycles are exposure capped and/or contain facies that formed below SWB. However, for conformable subtidal or peritidal cycles with facies deposited entirely above SWB, these estimates capture the maximum relative sea-level change, given the depths inferred for each facies.

Estimates of short-term relative sea-level change, in concert with variations in the types of cycle bounding surfaces, are indicative of different climate states and glacioeustatic forcing (Fig. 16G). In general, during times of low-amplitude glacioeustasy, basinward settings develop amalgamated conformable subtidal cycles that show minimal facies changes or may be noncyclic. In shoreward settings, carbonates usually fill accommodation space, creating flat-topped platforms with peritidal cycles that prograde extensively across the platform (Read et al., 1986; Read, 1995). Moderate- to high-amplitude relative sea-level changes should be recorded by (1) the juxtaposition of facies from markedly different water depths in the same cycle, and/or (2) subaerial exposure horizons developed on subtidal sediments. Basinward settings may record more conformable subtidal cycles with juxtaposed outer- and middle- to inner-platform facies, or disconformable subtidal cycles. In contrast, shoreward settings should record cycles capped by subaerial exposure horizons developed on inner-platform facies due to overall lowered accommodation coupled with forced regressions.

The record of relative sea-level change and cycle bounding surfaces is depicted in Figure 16. Four features are prominent and indicate shifts between intervals of high-amplitude and low-amplitude short-term relative sea-level fluctuations, including (1) a Chesterian (late Visean) onset of relative sea-level fluctuations of moderate to high amplitude; (2) a short-lived (earliest Morrowan or Bashkirian) dampening of relative sea-level changes and the development of peritidal cycle caps; (3) a return to high-amplitude, high-frequency relative sea-level changes in the mid-Morrowan (early Bashkirian) to mid-Desmoinesian (late Moscovian); and (4) a marked decrease in amplitude of late Desmoinesian to early Virgilian (Kasimovian to early Gzelian) relative sea-level fluctuations and a concomitant return to dominantly peritidal cycles.

Temporal Distribution of Climatic Signatures

Osagean and Meramecian (Visean) age strata contain ~65 m of noncyclic middle- to inner-ramp encrinites and ~15 m of photozoan inner-ramp facies. Low-amplitude relative sea-level changes are inferred because these strata contain only middle- to inner-ramp facies, with a long-lived noncyclic interval and conformable subtidal and peritidal cycles, lacking evidence for exposure of subtidal sediments. Meramecian strata likely exhibit autocyclic behavior because peritidal flat facies do not correlate regionally between Arrow Canyon and neighboring Battleship Wash (Bishop et al., 2009). Fenestral tidal flat facies suggest a subhumid climate for this time (e.g., Bova and Read, 1987; Hardie and Shinn, 1986).

The onset of moderate- to high-amplitude relative sea-level fluctuations occurs 1 m above the Meramecian-Chesterian (late Visean) boundary (Bishop et al., 2009), where subaerial exposure horizons are developed on subtidal encrinites and (stratigraphically higher) on middle- to outer-platform carbonates and siliciclastics (Figs. 5 and 8). In upper Chesterian (Serpukhovian)

cycles, exposure horizons developed on middle- to outer-ramp siliciclastic mudstones record changes in relative water depth at least equivalent to the depth of FWWB and likely SWB (>20–40 m; Fig. 16E). Notably, Chesterian Vertisols and calcic paleosols suggest that a seasonal dry subhumid to semiarid climate existed minimally by this time (Bishop et al., 2009).

Earliest Morrowan (earliest Bashkirian) strata exhibit evidence for a short-lived minimum in magnitudes of relative sea-level change (Figs. 16E, 16G). The lower ~20 m of Morrowan strata consist of mixed heterozoan-photozoan inner-ramp facies capped by thin tidal flat laminites; they contain only one thin (50 cm) incursion of outer-ramp facies (Fig. 9). The presence of tidal flats and rarity of outer-ramp facies suggest low-amplitude relative sea-level oscillations, during which the carbonate factory kept pace with transgressions, excluding outer-ramp facies, and tidal flat progradation kept pace with short-term regressions (Read et al., 1986; Read, 1995, 1998).

Mid-Morrowan to mid-Desmoinesian (early Bashkirian to Moscovian) strata record significantly higher-amplitude short-term sea-level changes (Figs. 16E, 16G). High-amplitude relative sea-level fluctuations are demonstrated where exposure horizons are developed on these dominantly outer-ramp cycles (Figs. 10–13). In addition, rapid sea-level changes are required by the short cycle durations in this interval. A tenfold decrease in average cycle duration occurs during the Atokan maximum in accommodation (Fig. 16C). In part, this decline in cycle duration reflects the ability of deeper water facies to record most high-amplitude sea-level changes, and thus minimize missed beats. However, some of the change in cycle duration likely also reflects changes in sea-level forcing (e.g., from the 100 k.y. eccentricity to the 40 k.y. obliquity band). Atokan strata include two caliches (Figs. 4F and 11) and a thick, reworked siliciclastic eolianite (at approximately A220), suggesting continuation of an overall dry subhumid to semiarid climate regime.

Relative sea-level changes diminished in amplitude during the late Pennsylvanian (Fig. 16). During a mid-Desmoinesian (upper Moscovian) transitional interval, amplitudes of relative water-depth change decrease markedly, yet middle- to inner-ramp cycles are bounded by subaerial exposure horizons (Fig. 14). These exposure-capped cycles suggest forced regressions under at least moderate-amplitude relative sea-level fluctuations. In addition, this interval likely corresponds to the development of a (rimmed) shelf to the west. This transition is recorded by the loss of storm-dominated outer- to middle-ramp facies, increasingly restricted, evaporative facies, common metazoan bioherms, and the slightly younger development of Missourian phyloid algal bioherms in western Nevada and Death Valley (Miller and Heller, 1994).

Upper Desmoinesian, Missourian, and lower Virgilian (uppermost Moscovian to lower Gzhelian) strata record a long-lived interval of low- to possibly moderate-amplitude relative sea-level fluctuations. These uniformly shallow-water, photozoan facies accumulated under approximately fourfold diminished accommodation. The low accommodation and shallow-water deposition require that any moderate or high-amplitude relative sea-level fluctuations would generate exposure-capped cycles. However, exposure horizons are rare—between 1 and 5 of 32 cycles, depending on whether truncation surfaces are interpreted as deflation surfaces. This suggests a long-lived interval of low-amplitude high-frequency sea-level changes, punctuated by rare moderate-amplitude sea-level changes. Given the rarity of exposure horizons and uniformly shallow, subtidal to peritidal facies, the range of relative sea-level change indicated in Figure 16 thus represents a maximum. The reappearance of common tidal flat-capped cycles further supports generally low-amplitude fluctuations, because even moderate sea-level falls would have caused shorelines to rapidly regress across the low-relief platform interior, stranding any tidal flats that might have formed during sea-level stillstands (e.g., Read et al., 1986; Read, 1995, 1998). The presence of cycles with thick (15 m) accumulations of highly restricted lagoonal dolomudstones at other times during this interval suggests the occurrence of sea-level changes of low to moderate amplitude; large enough to generate (possible) deflation surfaces in some cycles and to prevent tidal flat complexes from prograding across the highly restricted, shallow lagoons, but low enough to allow long-lived accumulation of these restricted facies without triggering facies changes. In addition, a Missourian calcisol, abundant concurrent dolomitization and evaporite emplacement (Fig. 3B), and a paucity of meteorically altered surfaces attest to a marked aridification during this time.

Upper Virgilian and Wolfcampian strata are heavily recrystallized, masking depositional and early diagenetic textures, and obscuring the relative sea-level record for this interval; therefore, environmental, sea-level, and climatic conditions are not interpreted from these strata.

Tectonic Control of Meter-Scale Cycles

It has been suggested that "jerky" subsidence or "yo-yo" tectonics might produce meter-scale peritidal cycles in proximity to faults (e.g., Cisne, 1986; Hardie et al., 1991). In particular, the forward stratigraphic models of De Bennedictis et al. (2007) suggest that in extensional settings, peritidal cycles might be produced in the hanging wall or graben by episodic downdrop (causing rapid deepening) followed by aggradation due to carbonate productivity. And disconformable subtidal cycles might be produced by episodic uplift of the footwall or horst (causing rapid shallowing and subaerial exposure horizons) followed by slow background subsidence, allowing the return of carbonate production. De Bennedictis et al. (2007) documented rates, frequencies, and magnitudes of slip that are consistent with many meter-scale carbonate cycles.

The Arrow Canyon record of high-amplitude relative sea-level change (disconformable subtidal cycles) would require high-frequency normal faulting with large slips (>40–50 m) that persisted over a very long period of mid-Mississippian to mid-Pennsylvanian time (~25 m.y.). However, this interval brackets several different tectonic regimes on the west coast of North America (Trexler et al., 1991, 2003, 2004; Stevens and Stone, 2007). In addition, such fault-controlled meter-scale cycles require depressed carbonate productivity to prevent "keep-up" peritidal conditions (during the interval of slow background subsidence), which would preclude deep subtidal facies. Otherwise, the resulting disconformable cycles would consist entirely of peritidal carbonate facies. Most important, Arrow Canyon disconformable subtidal cycles require both abrupt sea-level rises (commonly >40 m at the base of each cycle) and abrupt sea-level falls (because cycle thickness is much less than maximum recorded water depth), culminating in exposure of the platform. Such a relative sea-level history requires both forced transgressions and regressions, inconsistent with the structural model presented here. Moreover, the absence of seismites and growth faults and the relatively large (~200 km) distance from Arrow Canyon to the major Keeler basin fault system (Stevens and Stone, 2007) do not support a structural origin for these cycles. Rather, abundant evidence for coeval glaciation in Gondwanan records (see following discussion) implicates glacioeustatic forcing for these medium- to high-amplitude relative sea-level changes.

In contrast, intervals of low-amplitude relative sea-level change (dominantly peritidal and conformable subtidal cycles) are consistent with structural, autocyclic, or eustatic origins (e.g., Hardie et al., 1991; Burgess, 2001; De Bennedictis et al., 2007; Bosence et al., 2009). Regardless of the predominant

cause, however, such intervals cannot have been characterized by high amplitudes of glacioeustasy (see following).

Implications for Reconstructing the Late Paleozoic Record of Ice Volume

The paleo-tropical mixed carbonate-siliciclastic succession at Arrow Canyon provides substantial insights into Carboniferous low-latitude climate dynamics (Fig. 17). In other low-latitude settings, persistent high-amplitude (30 to >150 m) glacioeustasy throughout middle Mississippian to early Permian time has been extrapolated from the relief on unconformities and juxtaposed facies in cyclothems, and the geochemical records of their biotic components (e.g., Heckel, 1977, 1986, 1994; Adlis et al., 1988; Horbury, 1989; Soreghan and Giles, 1999a; Smith and Read, 2000; Wright and Vanstone, 2001; Cook et al., 2002; Joachimski et al., 2006). In contrast, high-latitude sedimentary records suggest multiple, smaller ice sheets that waxed and waned to varying degrees at different times, leading to alternating long-lived intervals of glacial maxima and minima (Isbell et al., 2003a, 2003b, 2008a, 2008b; Montañez et al., 2007; Fielding et al., 2008a, 2008b; Caputo et al., 2008). The low-latitude Arrow Canyon succession preserves a record of shifting modes of glacioeustasy that suggests a dynamic ice-volume history, consistent with the variable glaciation inferred from high latitudes. This conclusion demands a more nuanced view than the prevailing low-latitude model of persistent high-amplitude glacioeustasy caused by the protracted waxing and waning of a long-lived, geographically expansive late Paleozoic ice sheet.

In Arrow Canyon, basal Chesterian strata record the onset of high-amplitude relative sea-level fluctuations and inferred glacioeustasy (Bishop et al., 2009). This is slightly later than the onset of glaciogenic sedimentation in South America (Caputo et al., 2008), but predates evidence of glacial sedimentation elsewhere in Gondwana (Isbell et al., 2003a; Fielding et al., 2008a, 2008b). Tropical estimates for the onset of glacioeustasy range from late Meramecian (mid-Visean) to late Chesterian (late Serpukhovian) time but tend to converge near the base of the Chesterian (upper Visean) (Bishop et al., 2009). Variability in these records is likely due to differing subsidence regimes and positions on platforms, causing different sensitivities to eustatic sea-level changes, as well as possible limitations in biostratigraphic constraints and intercontinental correlation. Soon after the onset of glacioeustasy, repeated fluvial incision in the midcontinent suggests high-amplitude (>30–85 m) relative sea-level fluctuations (Smith and Read, 2000). In Arrow Canyon, a potentially long-lived disconformity occurs immediately above the Meramecian-Chesterian boundary (Bishop et al., 2009); this disconformity is interpreted to mask several of the high-amplitude glacioeustatic events inferred from the midcontinent (Bishop et al., 2009). Thus, the onset of glacioeustasy inferred from the Arrow Canyon succession is consistent with previously published near- and far-field records. This high-amplitude glacioeustasy continues until just above the Mississippian-Pennsylvanian boundary.

In lowermost Morrowan (lowermost Bashkirian) strata, common tidal flat cycle caps and a paucity of intercalated outer-ramp facies suggest a minor short-lived glacial minimum, or a large but stable ice sheet (DeConto and Pollard, 2003). This time period corresponds with an interval of normal fluvial and/or lacustrine sedimentation across eastern Australia (Fielding et al., 2008a, 2008b), which was near the polar circle at the time, more consistent with a time of limited glacial extent. Such short-lived minima have been attributed to fourth-order sea-level cycles superimposed on third-order sea-level highstands (Read, 1995), consistent with diminished glacioeustatic forcing during times of smaller ice sheets.

The mid-Morrowan to mid-Desmoinesian interval of inferred high-amplitude glacioeustasy is consistent with both low-latitude and high-latitude records, which suggest this as

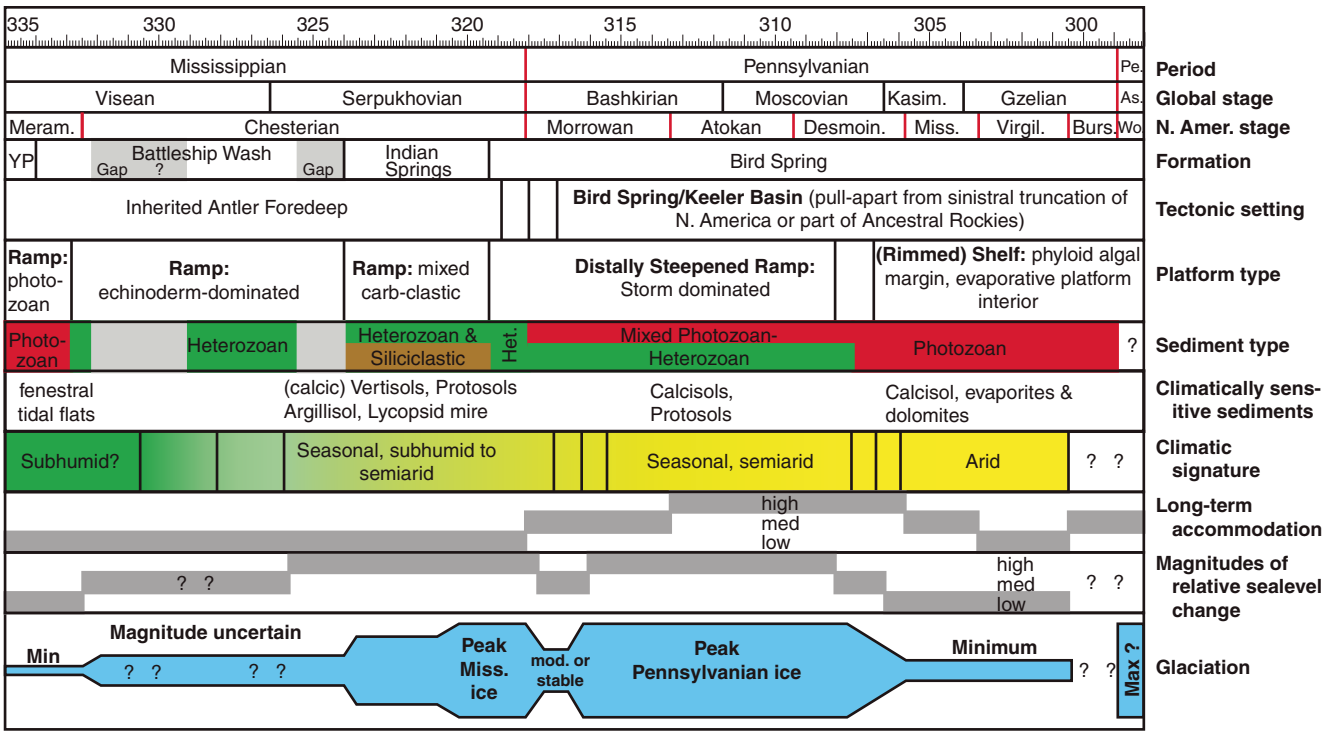

Figure 17. Summary of stratigraphic and climatic trends derived from Arrow Canyon record. Time scale after Gradstein et al. (2004).

a time of peak Carboniferous ice (e.g., Veevers and Powell, 1987; Frakes et al., 1992; Isbell et al., 2003a; Fielding et al., 2008a). In addition, the abundance of cherty heterozoan limestones with molds after sponge spicules, horizons with scattered phosphatized grains, and a subhumid to semiarid climate (see following) suggests upwelling of cool, nutrient-rich waters onto the Bird Spring platform during this interval (cf. Pope and Steffen, 2003).

Relative sea-level changes in upper Desmoinesian through lower Virgilian strata suggest an interval of significantly diminished magnitudes of relative sea-level fluctuations. It is during this interval, one traditionally attributed to peak icehouse conditions, that the greatest disparity exists between many near- and far-field records. In eastern Australia, late Pennsylvanian strata contain none of the glaciogenic sediments or evidence of high-amplitude relative sea-level fluctuations that typify other glacial intervals (Fielding et al., 2008a, 2008b, 2008c). Rather, these strata record normal marine and fluvial conditions, with only modest relative sea-level changes. Similarly, Antarctic records indicate nonglaciated basement highs on which thick paleosols developed and that were onlapped by postglacial strata (yet were not eroded by subsequent ice sheets), precluding the existence of a large ice sheet over Antarctica (Isbell et al., 2003a, 2003b, 2008b). These ice-free basins were polar, indicating a largely ice-free southern pole during this interval (Montañez et al., 2007; Fielding et al., 2008a, 2008b, 2008c; Isbell et al., 2008b). In subpolar settings, Desmoinesian to Virgilian ice is currently reported from several basins: the Paraná, Karoo-Kalahari, the Arabian Peninsula, and possibly the Congo (Rocha-Campos et al., 2008; Holtz et al., 2008; Isbell et al., 2003a, 2008a; Stollhofen et al., 2008; Martin et al., 2008). However, ice flow directions in these basins require multiple ice sheets (e.g., Isbell et al., 2008a), likely at least five to seven (J. Isbell, 2008, personal commun.). The absence of an ice sheet over Antarctica and eastern Australia and the presence of multiple smaller ice sheets in lower latitude basins place important constraints on continental ice sheet volume and possible amplitudes of glacioeustasy. Given the same aerial extent, multiple smaller ice centers can lock up significantly less water than one large ice sheet (Isbell et al., 2003a), leading to greatly dampened glacioeustasy. Thus, the late Pennsylvanian glacioeustatic minimum inferred from Arrow Canyon strata corresponds with a time of limited glacial extent in high-latitude Gondwana.

During the inferred upper Desmoinesian to lower Virgilian glacial minimum, other low-latitude records (e.g., midcontinent cyclothems) have traditionally been interpreted to reflect high-amplitude glacioeustasy. However, few of these interpretations are based on quantifiable evidence for sea-level change (e.g., erosional relief at lowstands). Rather, in upper Missourian to lower Virgilian strata, erosional relief on disconformities demonstrates only low- to moderate-amplitude (20–40 m) incision events (Feldman et al., 2005). Only two records suggest high-amplitude (60–70 m) sea-level fluctuations, based on fluvial incision at lowstands. Both intervals, however, occur just below the Desmoinesian-Missourian boundary (Schenk, 1967; Heckel et al., 1998). Furthermore, reexamination of some analogous later Virgilian "classic" incised valleys has resolved multiple superimposed lower-amplitude incision events, reducing inferred eustatic magnitudes from >60 m to <30 m (Fischbein et al., 2009).

The paradigm of high-amplitude late Desmoinesian to early Virgilian glacioeustasy is derived primarily from facies changes in Kansas-type cyclothems (Heckel, 1977, 1986, 1994; Boardman and Heckel, 1989). In these cyclothems, exposure horizons are juxtaposed against phosphatic black shales that accumulated below a pycnocline. The inferred depth of the pycnocline (>50–90 m) provides the fundamental constraint on relative sea-level change, leading to glacioeustatic estimates of >100 m (Heckel, 1977, 1994). This model is based on thermocline depths estimated from modern ocean basins, and requires the absence of any haloclines across the much more restricted midcontinent epeiric sea. However, such tropical seas would be highly sensitive to changes in runoff and the creation of shallow haloclines (e.g., Algeo and Heckel, 2008; Algeo et al., 2008). Indeed, the organic matter content and geochemistry of "core" shales in midcontinent cyclothems now support such a shallow (15–30 m) halocline (Algeo and Heckel, 2008). In addition, in the Visean paleo-equatorial Mount Head Group of Canada, glendonites (pseudomorphs after thinnolite) record near-freezing temperatures in shallow-marine facies, suggesting very shallow thermoclines in this tropical interior seaway (Brandley and Krause, 1994, 1997). In concert, this evidence for shallow (15–30 m) Carboniferous epeiric sea pycnoclines indicates that "core" shales might have formed at shallow depths and magnitudes of glacioeustasy may have been significantly less (~15–30 m) than commonly inferred.

In a similar fashion, high-amplitude (>70–120 m) glacioeustatic fluctuations have been reconstructed from oxygen isotopic changes within cyclothems (Adlis et al., 1988; Joachimski et al., 2006). Such estimates apply Quaternary open-ocean models of gentle thermoclines, absent haloclines, and buffered tropical climates (glacial-interglacial changes in sea-surface temperature of 1–4 °C) to Pennsylvanian shallow epeiric seas. However, these epeiric seas would have been especially prone to sluggish mixing of water masses (e.g., Holmden et al., 1998; Panchuk et al., 2005, 2006), large salinity fluctuations (e.g., >8 ppt across the Bahamas platforms; Patterson and Walter, 1994), shallow pycnoclines (Algeo and Heckel, 2008), and the development of subtle intrashelf depressions (e.g., where black shales form in shallow Mesozoic basins; Immenhauser and Scott, 2002; Homewood et al., 2008). For example, depleted $\delta^{18}O$ in conodont apatite deposited during highstands is interpreted to represent significantly diminished ice caps (Joachimski et al., 2006). However, interglacial temperature changes beyond the 2–4 ºC assumed by Joachimski et al. (2006) would have a significant effect on glacioeustatic estimates; e.g., an extra ~2 ºC cooling would offset 40–50 m of inferred sea-level change. Indeed, to the degree that such epeiric seas buffered continental temperatures, the seas' temperatures would have been perturbed (Stanley, 2006). Accordingly, evidence for near-freezing tropical surface waters (Brandley and Krause, 1994, 1997) and low-latitude low-altitude alpine glaciation (Soreghan et al., 2008) suggests a dynamic tropical climate with episodically cold, shallow waters. Joachimski et al. (2006) utilized a static salinity structure for the midcontinent sea, assuming no change between glacial and interglacial settings. This premise would be remarkable given the episodically stratified water column (punctuated by black shale deposition). Specifically, Joachimski et al. (2006) compared conodonts deposited nearshore during lowstands with those deposited offshore during highstands. Algeo and Heckel (2008) inferred salinity gradients of 10‰ within the stratified midcontinent epeiric sea, with highstand surface waters diluted by increased continental runoff. Using a modern equatorial Atlantic analog (Fairbanks et al., 1992), this salinity change would cause a 1‰ $\delta^{18}O$ depletion, offsetting ~100 m of inferred sea-level change (Joachimski et al., 2006). It might be argued that lateral salinity gradients would lead to lower salinity during lowstands due to deposition more proximal to the shoreline and presumed freshwater input. However, it is only during highstands in the midcontinent that evidence exists for stratified water columns (black shale deposition, rather than the stenohaline fauna and oxygenated bottom waters of transgressive and regressive limestones; Algeo and Heckel, 2008). Furthermore, midcontinent paleosols and coal deposits imply a

semiarid to subhumid climate during lowstands and a humid to subhumid climate during early transgressions, possibly sustained through highstands (e.g., DiMichelle et al., 2010, and references therein). Joachimski et al. (2006) assumed that the conodont-bearing organism did not respond to changing environmental conditions; however, there is much uncertainty regarding where in the water column conodont-hosting organisms lived and how they adapted to changing temperature, salinity, nutrient inputs, and oxygenation. Thus, the assumptions that modern thermocline profiles would be operable in late Pennsylvanian seas (Adlis et al., 1988), that glacial-interglacial tropical temperature changes in the Pennsylvanian were comparable to those of the Pleistocene (Joachimski et al., 2006), and that haloclines would not be operable, may be grossly oversimplified in these geochemical models.

Even within the Euramerican cyclothem record, a more nuanced interpretation is emerging. Rygel et al. (2008) compiled published estimates of glacioeustatic magnitudes; they showed that these reported estimates (of varying vintage and veracity) delineate broad patterns of fluctuating magnitudes through the late Paleozoic. More specifically, Heckel (2008) revisited his classic cyclothem interpretation to conclude that the majority of the late Pennsylvanian cyclothem record actually reflects highstands in long-term sea level and thus corresponds to diminished ice volume over Gondwana: these intervals include many of the major and intermediate cyclothems, for which the largest glacioeustatic magnitudes have been inferred. This analysis again reinforces that the cyclothems of the midcontinent, and the meter-scale cycles of Arrow Canyon, are not one size fits all, a simple repeated motif. Rather, they vary in character, and this variability reflects the dynamic nature of late Paleozoic glaciation.

Numerous authors have interpreted incision of 30–50 m in upper Virgilian carbonates (Wilson, 1967; Goldstein, 1988; Rankey et al., 1999), and Soreghan and Giles (1999a, 1999b) documented >30–85 m of relief on some unconformities. However, in Arrow Canyon, late Virgilian relative sea-level changes are difficult to interpret due to pervasive recrystallization, which obscures many depositional characteristics.

Aridification

The Arrow Canyon record indicates a marked aridification during the proposed late Pennsylvanian glacial minimum, a signature recorded elsewhere across equatorial western Pangea (Rankey, 1997; West et al., 1997; Olszewski and Patzkowski, 2003), equatorial eastern Pangea (DiMichele et al., 2009, and references therein), and high-latitude western Gondwana (Gulbranson et al., 2010). This late Pennsylvanian aridification is coincident with mass extinctions of tropical peat-forming lycopsids (DiMichelle and Phillips, 1996) and a concomitant change in the quality of Appalachian coal (Cecil et al., 2003).

It is commonly held that arid tropical conditions were coincident with icehouse intervals during the Paleozoic. This conclusion is largely based on extrapolating climate changes on short time scales ($<10^5$ yr; glacial-interglacial) based on Pleistocene analogues to longer time scales (10^6 yr; icehouse-greenhouse). Thus, evidence for arid glacials and humid interglacials has been extrapolated to require arid icehouse intervals and humid greenhouse intervals. In Permian time, however, aridification of the tropics was coincident with long-lived greenhouse intervals during the final phase of the late Paleozoic ice age (Montañez et al., 2007). During the late Pennsylvanian, aridification of western equatorial Pangea (and withdrawal of the epicontinental seas) has been linked to the final assembly of Pangea and thermotectonic buoyancy of the supercontinent, mechanisms independent of ice sheet dynamics (Veevers, 1994; Ziegler et al., 2002). However, this explanation is confounded by a marked aridification east of the main Pangean tropical mountain belt (DiMichele et al., 2009). Climate models suggest that aridification during glacial minima was caused by a weakening of Hadley cell convection and southward drift of the Intertropical Convergence Zone, leading to decreased precipitation levels and intensified monsoonal circulation across western equatorial Pangea (Poulsen et al., 2007; Montañez et al., 2007). In the Arrow Canyon record, the coincidence of significantly more arid conditions with the decline in amplitude of glacioeustasy argues for a strong component of climate forcing, suggesting a mechanistic link between pantropical aridification and the retreat of high-latitude Gondwanan ice sheets.

CONCLUSIONS

The record of glacioeustasy archived in Arrow Canyon requires a much more dynamic Carboniferous glaciation than commonly perceived. This record is at odds with the prevailing view that cyclothems require high-amplitude glacioeustasy throughout the ~50 m.y. interval of their deposition. The Arrow Canyon record is more consistent with high-latitude records that suggest alternating long-lived intervals of glacial maxima and minima, including a late Desmoinesian–early Virgilian glacial minimum. This late Pennsylvanian minimum was coincident with a marked aridification in Arrow Canyon and across the tropics, supporting a link between high-latitude ice sheet extent and stability and ocean-atmospheric dynamics in the tropics (e.g., Poulsen et al., 2007).

These climatic oscillations had a significant impact on the facies, cyclicity, and stacking patterns in Arrow Canyon. The recognition of a dynamic late Paleozoic ice age suggests that not all cyclothems formed under the same glacioeustatic forcing, and should lead to a much more nuanced understanding of late Paleozoic tropical sedimentation.

ACKNOWLEDGMENTS

We thank Mike Eros, Neil Kelley, and Erik Gulbranson for field assistance, and Paul Brenckle, Greg Wahlman, and Vladimir Davydov for biostratigraphic expertise. Blaine Cecil, Mitch Harris, Scott Ritter, and Lynn Soreghan provided advice and discussion. Scot Franklin, Tom Brady, James Sippell, Mark Boatwright, and Cathy Wiley all helped arrange access and sampling permits. We also thank Norm Winter and Greg Baxter for analytical and laboratory support. The clarity and focus of this manuscript were improved considerably by detailed reviews from Tom Algeo, Andrew Barnett, and associate editor Kate Giles. This work was supported by National Science Foundation grant EAR-0545654 (Sedimentary Geology and Paleontology Program) to Montañez.

APPENDIX A: BIOSTRATIGRAPHIC ZONATION IN ARROW CANYON

APPENDIX A. BIOSTRATIGRAPHIC ZONATION IN ARROW CANYON

Stages	Zone	Flora or fauna	Report, Reinterpretation	Meters, (A #), (bed number)
Late Meramecian	FU 8	*Apotognathus porcatus*	Brenckle (1997)	63
Basal Chesterian	Undifferentiated FU 9 and 10 (bilineatus)	Asteroarchaediscid foraminifers; *Gnathodus bilineatus, G. girtyi*	Brenckle (1997)	83
Basal Serpukhovian		*"Millerella" tortula*	Amoco: Groves and Miller, 2000; Bishop et al., 2009	88
Upper Serpukhovian	FU 12 (Unicornis)	*Adetognathodus unicornis*	Brenckle (1997); Brenckle et al. (1997); Lane et al. (1999)	101 (A0)
Upper Serpukhovian	FU 13 (Lower Muricatus)	*Rhachistognathus muricatus*	Lane et al. (1999)	148.6 (A31-1.1)
Upper Serpukhovian	FU 14 (Upper Muricatus)	*R. muricatus* and *Adetognathus lautus*	Lane et al. (1999)	173.7 (A48-0.7)
Basal Bashkirian	FU 15 (Noduliferus)	*Declinognathodus noduliferus*	Lane et al. (1999)	184.1 (A55-0.6)
Lower Bashkirian	Sinuatus-Minutus	*Idiognathoides sinuatus; Rhavhistognathus minutus minutus*	Baesemann and Lane (1985); Lane et al. (1999)	198.3 (A64-1.3)
Lower Bashkirian	Symmetricus	*Neognathodus symmetricus*	Baesemann and Lane (1985); Lane et al. (1999)	198.8 (A65-0.3)
Basal Atokan		*Pseudostaffella* and *Eoschubertella*	Amoco: Groves and Miller, 2000.; Baesemann and Lane (1985)	275 (A116)
Mid Atokan	Profusulinella	*Profusulinella spicata*	Cassity and Langenheim (1966); Amoco: Groves and Miller, 2000	436 (A223-0.5)
Basal Moscovian		*Profusulinella decora*	Amoco: Groves and Miller, 2000; V. Davydov, 2007, personal commun.	436.8 (A223-1.3)
Upper Atokan	Fusulinella	*Fusulinella*	Langenheim et al. (1984)	467.5 (A244-0.5)
Basal Desmoinesian		*Fusulina* (= *Beedeina*)	Webster (1969; Langenheim et al. (1984); Leavitt (2002)	525.5 (A283)
Desmoinesian:	Base of Lower Kittanning Cyclothem	various conodonts and foraminifera	Cecil et al. (2003); Stamm and Wardlaw (2003)	634 (A355-0.5)
Lowermost Kasimovian	N.A.	*Oketaella*	Amoco: Groves and Miller, 2000; V. Davydov, 2007, personal commun.	699 (A398-1.0)
Basal Missourian	N.A.	*Idiognathodus suciferus*	Leavitt (2002)	725 (A416)
Missourian	Tricites	*Triticites burgessae*	Cassity and Langenheim (1966)	752 (A434, bed 201)
Basal Virgilian	N.A.	*Pseudofusulinella utahensis, Triticites birdspringensis*	Amoco: Groves and Miller, 2000	820 (A479-0.5)
Basal Gzelian	N.A.	Approximates base of Virgilian	C.f., Stevens and Stone (2007)	820 (A479-0.5)
Basal Bursumian	N.A.	N.A.	Cassity and Langenheim (1966); G. Wahlman, 2006–2007, personal commun..	837.5 (A487)
Basal Asselian	N.A.	*Schwagerina*	Amoco: Groves and Miller, 2000	883 (A521-0.5)

Note: A# is Amoco (A prefix) location number; N.A.—not available. Stratigraphic height given in meters above the top of the Arrowhead Formation, the Amoco reference section (A# = 1.5 m) from the top of the Battleship Wash Formation, and the bed numbers of Cassity and Langenheim, 1966. Amoco data archived in university libraries is referenced as "Amoco: Groves and Miller, 2000," and is followed by a reference to any reinterpretation of those data.

REFERENCES CITED

Adlis, D.S., Grossman, E.L., Yancey, T.E., and McLerran, R.D., 1988, Isotope stratigraphy and paleodepth changes of Pennsylvanian cyclical sedimentary deposits: Palaios, v. 3, p. 487–506, doi: 10.2307/3514722.

Algeo, T.J., and Heckel, P.H., 2008, The Late Pennsylvanian Midcontinent Sea of North America: A review: Palaeogeography, Palaeoclimatology, Palaeoecology, v. 268, p. 205–221, doi: 10.1016/j.palaeo.2008.03.049.

Algeo, T.J., Heckel, P.H., Maynard, J.B., Blakey, R.C., and Rowe, H., 2008, Modern and ancient epicontinental seas and the superestuarine circulation model of marine anoxia, *in* Holmden, C., and Pratt, B.R., eds., Dynamics of epeiric seas: Sedimentological, paleontological and geochemical perspectives: Geological Association of Canada Special Publication 48, p. 7–38.

Baesemann, J.F., and Lane, H.R., 1985, Taxonomy and evolution of the genus *Rhachistognathus* Dunn (Conodonts: Late Mississippian to early Middle Pennsylvanian), *in* Lane, H.R., and Ziegler, W., eds., Toward a boundary in the middle of the Carboniferous: Stratigraphy and paleontology: Courier Forschunginstitut Senckenberg, v. 74, p. 93–135.

Barnett, A.J., and Wright, V.P., 2008, A sedimentological and cyclostratigraphic evaluation of the completeness of the Mississippian-Pennsylvanian (Mid-Carboniferous) Global Stratotype Section and Point, Arrow Canyon, Nevada, USA: Geological Society of London Journal, v. 165, p. 859–873, doi: 10.1144/0016-76492007-122.

Bishop, J.W., 2008, Sedimentation and diagenesis during the late Paleozoic ice age : Arrow Canyon, Nevada, and the Capitan Backreef, Slaughter Canyon, New Mexico [Ph.D. thesis]: Davis, University of California–Davis, 244 p.

Bishop, J.W., Montañez, I.P., Gulbranson, E.L., and Brenckle, P.L., 2009, The onset of mid-Carboniferous glacio-eustasy: Sedimentologic and diagenetic constraints, Arrow Canyon, NV: Palaeogeography, Palaeoclimatology, Palaeoecology, v. 276, p. 217–243, doi: 10.1016/j.palaeo.2009.02.019.

Blakey, R.C., 2007, Carboniferous-Permian paleogeography of the assembly of Pangaea, *in* Wong, T.E., ed., Proceedings of the XVth International Congress on Carboniferous and Permian Stratigraphy. Utrecht, 10–16 August 2003: Amsterdam, Royal Dutch Academy of Arts and Sciences, p. 443–356.

Boardman, D.R., II, and Heckel, P.H., 1989, Glacial-eustatic sea-level curve for early Late Pennsylvanian sequence in north-central Texas and biostratigraphic correlation with curve for mid-continent North America: Geology, v. 17, p. 802–805, doi: 10.1130/0091-7613(1989)017<0802:GESLCF>2.3.CO;2.

Bosence, D., Procter, E., Aurell, M., Kahla, A.B., Boudagher-Fadel, M., Casaglia, F., Cirilli, S., Mehdie, M., Nieto, L., Rey, J., Scherreiks, R., Soussi, M., and Waltham, D., 2009, A dominant tectonic signal in high-frequency, peritidal carbonate cycles? A regional analysis of Liassic platforms from Western Tethys: Journal of Sedimentary Research, v. 79, p. 389–415, doi: 10.2110/jsr.2009.038.

Bova, J.A., and Read, J.F., 1987, Incipiently drowned facies within a cyclic peritidal continental ramp sequence: Chepultepec interval, Virginia Appalachians: Geological Society of America Bulletin, v. 98, p. 714–727, doi: 10.1130/0016-7606(1987)98<714:IDFWAC>2.0.CO;2.

Brandley, R.T., and Krause, F.F., 1994, Thinolite-type pseudomorphs after ikaite: Indicators of cold water on the subequatorial western margin of Lower Carboniferous North America, *in* Beauchamp, B., et al., eds., Pangea: Global environments and resources: Canadian Society of Petroleum Geologists Memoir 17, p. 333–344.

Brandley, R.T., and Krause, F.F., 1997, Upwelling, thermoclines and wave-sweeping on an equatorial carbonate ramp: Lower Carboniferous strata of western Canada, *in* James, N.P., and Clarke, J.A.D., eds., Cool-water carbonates: SEPM (Society for Sedimentary Geology) Special Publication 56, p. 365–390.

Brenckle, P.L., 1997, Battleship Wash section. Paleoforams '97 Guidebook: Post-conference field trip to the Arrow Canyon Range, Southern Nevada U.S.A.: Cushman Foundation Foraminiferal Research, Supplement to Special Publication 36, p. 45–53.

Brenckle, P.L., Baesemann, J.F., Lane, H.R., West, R.R., Webster, G.D., Langenheim, R.L., Brand, U., and Richards, B.C., 1997, Arrow Canyon, the mid-Carboniferous boundary stratotype: Cushman Foundation Foraminiferal Research, Supplement to Special Publication 36, p. 45–53.

Burgess, P.M., 2001, Modeling carbonate sequence development without relative sea-level oscillations: Geology, v. 29, p. 1127–1130, doi: 10.1130/0091-7613(2001)029<1127:MCSDWR>2.0.CO;2.

Caputo, M.V., de Melo, J.H.G., Streel, M., and Isbell, J.L., 2008, Late Devonian and Early Carboniferous glacial records of South America, *in* Fielding, C.R., eds., Resolving the late Paleozoic ice age in time and space: Geological Society of America Special Paper 441, 161–174.

Cassity, P.E., and Langenheim, R.L., Jr., 1966, Pennsylvanian and Permian fusulinids of the Bird Spring Group from Arrow Canyon, Clark County, Nevada: Journal of Paleontology, v. 40, p. 931–968.

Cecil, C.B., Dulong, F.T., West, R.R., Stamm, R., Wardlaw, B., and Edgar, N.T., 2003, Climate controls on the stratigraphy of a Middle Pennsylvanian cyclothem in North America, *in* Cecil, C.B., and Edgar, T.N., eds., Climate controls on stratigraphy: SEPM (Society for Sedimentary Geology) Special Publication 77, p. 151–182.

Cisne, J.L., 1986, Earthquakes recorded stratigraphically on carbonate platforms: Nature, v. 323, p. 320–322, doi: 10.1038/323320a0.

Cook, H.E., Zhemchuzhnikov, V.G., Zempolich, W.G., Zhaimina, V.Y., Buvtyshkin, V.M., Kotova, E.A., Golub, L.Y., Zorin, A.Y., Lehmann, P.J., Alexeiev, D.V., Giovanneli, A., Viaggi, M., Fretwell, N., Lapointe, P., and Corboy, J.J., 2002, Devonian and Carboniferous carbonate platform facies in the Bolshoi Karatau, southern Kazakhstan: Outcrop analogs for coeval carbonate oil and gas fields in the North Caspian Basin, western Kazakhstan, *in* Zempolich, W.G., and Cook, H.E., eds., Paleozoic carbonates of the Commonwealth of Independent States (CIS): Subsurface reservoirs and outcrop analogs: SEPM (Society for Sedimentary Geology) Special Publication 74, p. 81–122.

De Benedictis, D., Bosence, D., and Waltham, D., 2007, Tectonic control on peritidal carbonate parasequence formation: An investigation using forward tectono-stratigraphic modeling: Sedimentology, v. 54, p. 587–605, doi: 10.1111/j.1365-3091.2006.00851.x.

DeConto, R.M., and Pollard, D., 2003, A coupled climate-ice sheet modeling approach to the early Cenozoic history of the Antarctic ice sheet: Palaeogeography, Palaeoclimatology, Palaeoecology, v. 198, p. 39–52, doi: 10.1016/S0031-0182(03)00393-6.

Dickinson, W.R., 2006, Geotectonic evolution of the Great Basin: Geosphere, v. 2, p. 353–368, doi: 10.1130/GES00054.1.

Dickson, J.A.D., 1965, A modified staining technique for carbonates in thin section: Nature, v. 205, p. 587, doi: 10.1038/205587a0.

DiMichelle, W.A., and Phillips, T.L., 1996, Climate change, plant extinctions and vegetational recovery during the Middle-Late Pennsylvanian transition: The case of tropical peat-forming environments in North America, *in* Hart, M.B., ed., Biotic recovery from mass extinction events: Geological Society of America Special Publication 102, p. 201–221.

DiMichele, W.A., Montañez, I.P., Poulsen, C.J., and Tabor, N.J., 2009, Climate and vegetational regime shifts in the late Paleozoic ice age earth: Geobiology, v. 7, p. 200–226, doi: 10.1111/j.1472-4669.2009.00192.x.

DiMichele, W.A., Cecil, C.B., Montañez, I.P., and Falcon-Lang, H., 2010, Cyclic changes in middle and late Pennsylvanian-age paleoclimate and floristic dynamics in tropical Pangaea: International Journal of Coal Geology (in press).

Dunham, R.J., 1969, Vadose pisolites in the Capitan Reefs (Permian) New Mexico and Texas, *in* Friedman, G.M., ed., Depositional environments in carbonate rocks: Society of Economic Paleontologists and Mineralogists Special Publication 14, p. 182–191.

Dunham, R.J., 1971, Meniscus cement, *in* Bricer, O.P., ed., Carbonate cements: Johns Hopkins University Studies in Geology, v. 19, p. 297–300.

Ellwood, B.B., Tomkin, J.H., Richards, B.C., Benoist, S.L., and Lambert, L.L., 2007, MSEC data sets record glacially driven cyclicity: Examples from the arrow canyon Mississippian-Pennsylvanian GSSP and associated sections: Palaeogeography, Palaeoclimatology, Palaeoecology, v. 255, p. 377–390, doi: 10.1016/j.palaeo.2007.08.006.

Elrick, M., and Read, J.F., 1991, Cyclic ramp to basin carbonate deposits, Lower Mississippian, Wyoming and Montana: A combined field and computer modeling study: Journal of Sedimentary Petrology, v. 61, p. 1194–1224.

Fairbanks, R.G., Charles, C.D., and Wright, J.D., 1992, Origin of global meltwater pulses, *in* Taylor, R.E., ed., Radiocarbon after four decades: New York, Springer, p. 473–500.

Feldman, H.R., Franseen, E.K., Joeckel, R.M., and Heckel, P.H., 2005, Impact of longer-term modest climate shifts on architecture of high-frequency sequences (cyclothems), Pennsylvanian of Midcontinent U.S.A: Journal of Sedimentary Research, v. 75, p. 350–368, doi: 10.2110/jsr.2005.028.

Fielding, C.R., Frank, T.D., Birgenheier, L.P., Rygel, M.C., Jones, A.T., and Roberts, J., 2008a, Stratigraphic imprint of the late Palaeozoic ice age in eastern Australia: A record of alternating glacial and non-glacial climate regime: Geological Society of London Journal, v. 165, p. 129–140, doi: 10.1144/0016-76492007-036.

Fielding, C.R., Frank, T.D., Birgenheier, L.P., Rygel, M.C., Jones, A.T., and Roberts, J., 2008b, Stratigraphic record and facies associations of the late Paleozoic ice age in eastern Australia (New South Wales and Queensland), *in* Fielding, C.R., et al., eds., Resolving the late Paleozoic ice age in time and space: Geological Society of America Special Paper 441, p. 41–58.

Fielding, C.R., Frank, T.D., and Isbell, J.L., 2008c, The late Paleozoic ice age—A review of current understanding and synthesis of global climate patterns, *in* Fielding, C.R., et al., eds., Resolving the late Paleozoic ice age in time and space: Geological Society of America Special Paper 441, p. 343–443.

Fischbein, S.A., Joeckel, R.M., and Fielding, C.R., 2009, Fluvial-estuarine reinterpretation of large, isolated sandstone bodies in epicontinental cyclothems, Upper Pennsylvanian, northern Midcontinent, USA, and their significance for understanding late Paleozoic sea-level fluctuations: Sedimentary Geology, v. 216, p. 15–28, doi: 10.1016/j.sedgeo.2009.01.009.

Foster, M.S., Riosmena-Rodriguez, R., Steller, D.L., and Woelkerling, W.J., 1997, Living rhodolith beds in the Gulf of California and their implications for paleoenvironmental interpretation, *in* Johnson, M.E., and Ledesma-Vázquez, J., eds., Pliocene carbonates and related facies flanking the Gulf of California, Baja California, Mexico: Geological Society of America Special Paper 318, p. 127–140.

Frakes, L.A., Francis, J.E., and Syktus, J.L., 1992, Climate modes of the Phanerozoic: The history of the Earth's climate over the past 600 million years: Cambridge, Cambridge University Press, 286 p.

Galonka, J., and Kiessling, W., 2002, Phanerozoic time scalel and definition of time slices, *in* Kiessling, W., et al., eds., Phanerozoic reef patterns: SEPM (Society for Sedimentary Geology) Special Publication 72, p. 11–20.

Gibling, M.R., and Giles, P.S., 2005, Rhythmic upper Paleozoic strata of Euramerica: Equatorial indicators

of Gondwanan glaciation?: Geological Society of America Abstracts with Programs, v. 37, no. 7, p. 255.

Gischler, E., and Lomando, A.J., 2005, Offshore sedimentary facies of a modern carbonate ramp, Kuwait, northwestern Arabian-Persian Gulf: Facies, v. 50, p. 443–462, doi: 10.1007/s10347-004-0027-4.

Goldstein, R.H., 1988, Paleosols of Late Pennsylvanian cyclic strata, New Mexico: Sedimentology, v. 35, p. 777–803, doi: 10.1111/j.1365-3091.1988.tb01251.x.

Gong, S.Y., Mii, H.S., Wei, K.Y., Horng, C.S., You, C.F., Huang, F.W., Chi, W.R., Yui, T.F., Torng, P.K., Huang, S.T., Wang, S.W., Wu, J.C., and Yang, K.M., 2005, Dry climate near the Western Pacific Warm Pool: Pleistocene caliches of the Nansha Islands, South China Sea: Palaeogeography, Palaeoclimatology, Palaeoecology, v. 226, p. 205–213, doi: 10.1016/j.palaeo.2005.05.012.

Gradstein, F., Ogg, J.G., and Smith, A.G., 2004, A geologic time scale 2004: Cambridge, Cambridge University Press, 610 p.

Groves, J.R., and Miller, M.A., 2000, Donation of Amoco fossil collections: Journal of Paleontology, v. 74, no. 6, p. 1196–1197.

Gulbranson, E.L., Montañez, I.P., Schmitz, M.D., Limarino, C.O., Isbell, J.L., Marenssi, S.A., and Crowley, J.L., 2010, High-resolution U-Pb calibration of Carboniferous glacigenic deposits, Rio Blanco and Paganzo basins, northwest Argentina: Geological Society of America Bulletin (in press).

Hagan, G.M., and Logan, B.W., 1974, Development of carbonate banks and hypersaline basins, Shark Bay, Western Australia, *in* Logan, B.W., et al., eds., Evolution and diagenesis of Quaternary carbonate sequences, Shark Bay, Western Australia: American Association of Petroleum Geologists Memoir 22, p. 61–139.

Hardie, L.A., and Shinn, E.A., 1986, Carbonate depositional environments, Part 3: Tidal flats: Colorado School of Mines Quarterly, v. 81, p. 59–74.

Hardie, L.A., Dunn, P.A., and Goldhammer, R.K., 1991, Field and modeling studies of Cambrian carbonate cycles, Virginia Appalachians—A discussion: Journal of Sedimentary Petrology, v. 61, p. 636–646.

Harris, P.M., 1979, Facies anatomy and diagenesis of a Bahamian ooid shoal, *in* Ginsberg, R.N., ed., Sedimenta VII: Miami, Florida, Comparative Sedimentology Lab, 164 p.

Heckel, P.H., 1977, Origin of phosphatic black shale facies in Pennsylvanian cyclothems of mid-continent North America: American Association of Petroleum Geologists Bulletin, v. 61, p. 1045–1068.

Heckel, P.H., 1986, Sea-level curve for Pennsylvanian eustatic marine transgressive-regressive depositional cycles along mid-continent outcrop belt, North America: Geology, v. 14, p. 330–334, doi: 10.1130/0091-7613(1986)14<330:SCFPEM>2.0.CO;2.

Heckel, P.H., 1994, Evaluation of evidence for glacio-eustatic control over marine Pennsylvanian cyclothems in North America and consideration of possible tectonic effects, *in* Dennison, J.M., and Ettensohn, F.R., eds., Tectonic and eustatic controls on sedimentary cycles: SEPM (Society for Sedimentary Geology) Concepts in Sedimentology and Paleontology Series 4, p. 65–87.

Heckel, P.H., 2002, Genetic stratigraphy and conodont biostratigraphy of upper Desmoinesian–Missourian (Pennsylvanian) cyclothem succession in Midcontinent North America, *in* Hills, L.V., et al., eds., The Carboniferous and Permian of the world: Canadian Society of Petroleum Geologists Memoir 19, p. 99–119.

Heckel, P.H., 2008, Pennsylvanian cyclothems in Midcontinent North America as far-field effects of waxing and waning of Gondwana ice sheets, *in* Fielding, C.R., et al., eds., Resolving the late Paleozoic ice age in time and space: Geological Society of America Special Paper 441, 275–290.

Heckel, P.H., Gibling, M.R., and King, N.R., 1998, Stratigraphic model for glacial-eustatic Pennsylvanian cyclothems in highstand nearshore detrital regimes: Journal of Geology, v. 106, p. 373–383, doi: 10.1086/516030.

Heckel, P.H., Alekseev, A.S., Barrick, J.E., Boardman, D.R., Goreva, N.V., Nemryovska, T.I., Ueno, K., Villa, E., and Work, D.M., 2007, Cyclothem ["digital"] correlation and biostratigraphy across the global Moscovian-Kasimovian-Gzhelian stage boundary interval (Middle-Upper Pennsylvanian) in North America and eastern Europe: Geology, v. 35, p. 607–610, doi: 10.1130/G23564A.1.

Holmden, C., Creaser, R.A., Muehlenbachs, K., Leslie, S.A., and Bergstrom, S.M., 1998, Isotopic evidence for geochemical decoupling between ancient epeiric seas and bordering oceans: Implications for secular curves: Geology, v. 26, p. 567–570, doi: 10.1130/0091-7613(1998)026<0567:IEFGDB>2.3.CO;2.

Holtz, M., Souza, P.A., and Iannuzzi, R., 2008, Sequence stratigraphy and biostratigraphy of the late Carboniferous to Early Permian glacial succession (Itararé subgroup) at the eastern-southeastern margin of the Paraná Basin, Brazil, *in* Fielding, C.R., et al., eds., Resolving the late Paleozoic ice age in time and space: Geological Society of America Special Paper 441, 115–130.

Homewood, P., Razin, P., Grélaud, C., Droste, H., Vahrenkamp, V., Mettraux, M., and Mattner, J., 2008, Outcrop sedimentology of the Natih Formation, northern Oman: A field guide to selected outcrops in the Adam Foothills and Al Jabal al Akhdar areas: Geoarabia, v. 13, p. 39–120.

Horbury, A.D., 1989, The relative roles of tectonism and eustasy in the deposition of the Urswick Limestone in south Cumbria and north Lancashire, *in* Arthurton, R.S., et al., eds., The role of tectonics in Devonian and Carboniferous sedimentation in the British Isles: Yorkshire Geological Society Occasional Publication 6, p. 253–269.

Horton, D.E., Poulsen, C.J., and Pollard, D., 2007, Orbital and CO_2 forcing of late Paleozoic continental ice sheets: Geophysical Research Letters, v. 34, L19708, doi: 10.1029/2007GL031188.

Immenhauser, A., and Scott, R.W., 2002, An estimate of Albian sea-level amplitudes and its implications for the duration of stratigraphic hiatuses: Sedimentary Geology, v. 152, p. 19–28, doi: 10.1016/S0037-0738(02)00260-9.

Isbell, J.L., Miller, M.F., Wolfe, K.L., and Lenaker, P.A., 2003a, Timing of late Paleozoic glaciation in Gondwana: Was glaciation responsible for the development of northern hemisphere cyclothems?, *in* Chan, M.A., and Archer, A.W., eds., Extreme depositional environments: Mega end members in geologic time: Geological Society of America Special Paper 370, p. 5–24.

Isbell, J.L., Lenaker, P.A., Askin, R.A., Miller, M.F., and Babcock, L.E., 2003b, Reevaluation of the timing and extent of late Paleozoic glaciation in Gondwana: Role of Transantarctic Mountains: Geology, v. 31, p. 977–980, doi: 10.1130/G19810.1.

Isbell, J.L., Cole, D.I., and Catuneanu, O., 2008a, Carboniferous-Permian glaciation in the main Karoo Basin, South Africa: Stratigraphy, depositional controls, and glacial dynamics, *in* Fielding, C.R., et al., eds., Resolving the late Paleozoic ice age in time and space: Geological Society of America Special Paper 441, 71–82.

Isbell, J.L., Kosch, Z.J., Szablewski, G.M., and Lenaker, P.A., 2008b, Permian glacigenic deposits in the Transantarctic Mountains, Antarctica, *in* Fielding, C.R., et al., eds., Resolving the late Paleozoic ice age in time and space: Geological Society of America Special Paper 441, 59–70.

James, N.P., 1997, The cool-water carbonate depositional realm, *in* James, N.P., and Clarke, J.A.D., eds., Cool-water carbonates: SEPM (Society for Sedimentary Geology) Special Publication 56, p. 1–20.

Joachimski, M.M., von Bitter, P.H., and Buggisch, W., 2006, Constraints on Pennsylvanian glacioeustatic sea-level changes using oxygen isotopes of conodont apatite: Geology, v. 34, p. 277–280, doi: 10.1130/G22198.1.

Kammer, T.W., and Ausich, W.I., 2006, The "Age of Crinoids": A Mississippian biodiversity spike coincident with widespread carbonate ramps: Palaios, v. 21, p. 238–248, doi: 10.2110/palo.2004.p04-47.

Kendall, C.G.S.C., and Skipwith, P.A.D.E., 1969, Holocene shallow-water carbonate and evaporite sediments of Khor al Bazam, Abu Dhabi, southwest Persian Gulf: American Association of Petroleum Geologists Bulletin, v. 53, p. 841–869.

Kluth, C.F., 1986, Plate tectonics of the Ancestral Rocky Mountains, *in* Peterson, J.A., ed., Paleotectonics and sedimentation in the Rocky Mountain region, United States: American Association of Petroleum Geologists Memoir 41, p. 353–369.

Kluth, C.F., and Coney, P.J., 1981, Plate tectonics of the Ancestral Rocky Mountains: Geology, v. 9, p. 10–15, doi: 10.1130/0091-7613(1981)9<10:PTOTAR>2.0.CO;2.

Lane, H.R., Brenckle, P.L., Baesemann, J.F., and Richards, B.C., 1999, The IUGS boundary in the middle of the Carboniferous: Arrow Canyon, Nevada, USA: Episodes, v. 22, p. 272–283.

Langenheim, R.L., Webster, G.D., and Weibel, C.P., 1984, Atokan rocks of the Bird Spring Group, Arrow Canyon, Clark County, Nevada: Oklahoma Geological Survey Bulletin, v. 136, p. 133–156.

Leavitt, A.J., 2002, Stratigraphic architecture of mid-ramp, icehouse carbonates: A case study from Desmoinesian strata (Middle Pennsylvanian) of Arrow Canyon, southern Nevada: [M.S. thesis]: Provo, Utah, Brigham Young University, 52 p.

Lehmann, C., Osleger, D.A., and Montañez, I.P., 1998, Controls on cyclostratigraphy of lower Cretaceous carbonates and evaporites, Cupido and Coahuila platforms, northeastern Mexico: Journal of Sedimentary Research, v. 68, p. 1109–1130.

Lehmann, C., Osleger, D.A., and Montañez, I.P., 2000, Sequence stratigraphy of Lower Cretaceous (Barremian-Albian) carbonate platforms of northeastern Mexico: Regional and global correlations: Journal of Sedimentary Research, v. 70, p. 373–391, doi: 10.1306/2DC40917-0E47-11D7-8643000102C1865D.

Logan, B.W., Harding, J.L., Ahr, W.M., Williams, J.D., and Snead, R.G., 1969, Carbonate sediments and reefs, Yucatan shelf, Mexico: American Association of Petroleum Geologists Memoir 11, 198 p.

Logan, B.W., Davies, G.R., Read, J.F., and Cebulski, D.E., eds., 1970, Carbonate sedimentation and environments, Shark Bay, Western Australia: American Association of Petroleum Geologists Memoir 13, 37 p.

Loreau, J.P., and Purser, B.H., 1973, Distribution and ultrastructure of Holocene ooids in the Persian Gulf, *in* Purser, B.H., ed., The Persian Gulf: New York, Springer-Verlag, p. 279–328.

Machette, M.N., 1985, Calcic soils of the south-western United States, *in* Weide, D.L., ed., Soils and Quaternary geology of the southwestern United States: Geological Society of America Special Paper 203, p. 1–21.

Mack, G.H., James, W.C., and Monger, H.C., 1993, Classification of paleosols: Geological Society of America Bulletin, v. 105, p. 129–136, doi: 10.1130/0016-7606(1993)105<0129:COP>2.3.CO;2.

Martin, J.R., Redfern, J., and Aitken, J.F., 2008, A regional overview of the late Paleozoic glaciation in Oman, *in* Fielding, C.R., et al., eds., Resolving the late Paleozoic ice age in time and space: Geological Society of America Special Paper 441, 161–174.

Melim, L.A., Westphal, J., Swart, P.K., Eberli, G.P., and Munnecke, A., 2002, Questioning carbonate diagenetic paradigms: evidence from the Neogene of the Bahamas: Marine Geology, v. 185, p. 27–54, doi: 10.1016/S0025-3227(01)00289-4.

Miller, R.P., and Heller, P.L., 1994, Depositional framework and controls on mixed carbonate-siliciclastic gravity flows: Pennsylvanian-Permian shelf to basin transect, southwestern Great Basin, USA: Sedimentology, v. 41, p. 1–20, doi: 10.1111/j.1365-3091.1994.tb01389.x.

Montañez, I.P., and Osleger, D.A., 1993, Parasequence stacking patterns, third-order accommodation events and sequence stratigraphy of Middle to Upper Cambrian platform carbonates, Bonanza King Formation, southern Great Basin, *in* Loucks, R.G., and Sarg, F.R., eds., Carbonate sequence stratigraphy: Recent developments and applications: American Association of Petroleum Geologists Memoir 57, p. 305–326.

Montañez, I.P., and Osleger, D.A., 1996, Contrasting sequence boundary zones developed within cyclic carbonates of the Bonanza King Formation, Middle to Late Cambrian, southern Great Basin, *in* Witzke, B.J., et al., eds., Paleozoic sequence stratigraphy: Views from the North American craton. Geological Society of America Special Paper 306, p. 7–22.

Montañez, I.P., and Read, J.F., 1992a, Eustatic control on early dolomitization of cyclic peritidal carbonates: Evidence from the Early Ordovician Upper Knox Group, Appalachians: Geological Society of America Bulletin, v. 104, p. 872–886, doi: 10.1130/0016-7606(1992)104<0872:ECOEDO>2.3.CO;2.

Montañez, I.P., and Read, J.F., 1992b, Fluid-rock interaction history during stabilization of early dolomites of the Upper Knox Group (Early Ordovician), Appalachians: Journal of Sedimentary Petrology, v. 62, p. 753–778.

Montañez, I.P., Tabor, N.J., Niemeier, D., DiMichele, W.A., Frank, T.D., Fielding, C.R., Isbell, J.L., Birgenheier, L.P., and Rygel, M.C., 2007, Vegetation instability during late Paleozoic deglaciation: Science, v. 315, p. 87–91, doi: 10.1126/science.1134207.

Olszewski, T.D., and Patzkowski, M.E., 2003, From cyclothems to sequences: The record of eustasy and climate on an icehouse epeiric platform (Pennsylvanian-Permian, North American Midcontinent): Journal of Sedimentary Research, v. 73, p. 15–30.

Osleger, D.A., and Read, J.F., 1991, Relation of eustasy to stacking patterns of meter-scale carbonate cycles, Late Cambrian, U.S.A: Journal of Sedimentary Petrology, v. 61, p. 1225–1252.

Page, W.R., and Dixon, G.L., 1997, Geologic framework of the Arrow Canyon area, Clark County, Nevada: Cushman Foundation Foraminiferal Research, Supplement to Special Publication 36, p. 5–12.

Panchuk, K.M., Holmden, C., and Kump, L.R., 2005, Sensitivity of the epeiric sea carbon isotope record to local-scale carbon cycle processes: Tales from the Mohawkian Sea: Palaeogeography, Palaeoclimatology, Palaeoecology, v. 228, p. 320–337, doi: 10.1016/j.palaeo.2005.06.019.

Panchuk, K.M., Holmden, C.E., and Leslie, S.A., 2006, Local controls on carbon cycling in the Ordovician mid-continent region of North America, with implications for carbon isotope secular curves: Journal of Sedimentary Research, v. 76, p. 200–211, doi: 10.2110/jsr.2006.017.

Patterson, W.P., and Walter, L.M., 1994, Depletion of ^{13}C in seawater ΣCO_2 on modern carbonate platforms: significance for the carbon isotope record of carbonates: Geology, v. 22, p. 885–888, doi: 10.1130/0091-7613(1994)022<0885:DOCISC>2.3.CO;2.

Pierce, R.W., and Langenheim, R.L., Jr., 1972, Platform condonts of the Monte Cristo Group, Mississippian, Arrow Canyon Range, Clark Country, Nevada: Journal of Paleontology, v. 48, p. 149–169.

Poole, F.G., and Sandberg, C.A., 1991, Mississippian paleogeography and conodont biostratigraphy of the western United States, *in* Cooper, J.D., and Stevens, C.H., eds., Paleozoic paleogeography of the Western United States–II: Pacific Section SEPM (Society for Sedimentary Geology) Publication 67, p. 107–136.

Pope, M.C., and Steffen, J.B., 2003, Widespread, prolonged late Middle to Late Ordovician upwelling in North America: A proxy record of glaciation?: Geology, v. 31, p. 63–66, doi: 10.1130/0091-7613(2003)031<0063:WPLMTL>2.0.CO;2.

Poulsen, C.J., Pollard, D., Montañez, I.P., and Rowley, D., 2007, Late Paleozoic tropical climate response to Gondwanan deglaciation: Geology, v. 35, p. 771–774, doi: 10.1130/G23841A.1.

Purser, B.H., and Evans, G., 1973, Regional sedimentation along the Trucial Coast, SE Persian Gulf, *in* Purser, B.H., ed., The Persian Gulf: New York, Springer-Verlag, p. 211–231.

Purser, B.H., and Seibold, E., 1973, The principal environmental factors influencing Holocene sedimentation and diagenesis in the Persian Gulf, *in* Purser, B.H., ed., The Persian Gulf: New York, Springer-Verlag, p. 1–10.

Rankey, E.C., 1997, Relations between relative changes in sea level and climate shifts: Pennsylvanian-Permian mixed carbonate-siliciclastic strata, western United States: Geological Society of America Bulletin, v. 109, p. 1089–1100, doi: 10.1130/0016-7606(1997)109<1089:RBRCIS>2.3.CO;2.

Rankey, E.C., Bachtel, S.L., and Kaufman, J., 1999, Controls on stratigraphic architecture of icehouse mixed carbonate-siliciclastic systems: A case study from the Holder Formation (Pennsylvanian, Virgilian), Sacramento Mountains, New Mexico, *in* Harris, P.M., et al., eds., Recent advances in carbonate sequence stratigraphy: Application to reservoirs, outcrops, and models: SEPM (Society for Sedimentary Geology) Special Publication 63, p. 127–150.

Read, J.F., 1985, Carbonate platform facies models: American Associate of Petroleum Geologists Bulletin, V. 69, p. 1–21.

Read, J.F., 1995, Overview of carbonate platform sequences, cycle stratigraphy and reservoirs in greenhouse and icehouse worlds, *in* Read, J.F., et al., eds., Milankovitch sea level changes, cycles and reservoirs on carbonate platforms in greenhouse and icehouse worlds: SEPM (Society for Sedimentary Geology) Short Course Notes 35, p. 1–102.

Read, J.F., 1998, Phanerozoic carbonate ramps from greenhouse, transitional and ice-house worlds: Clues from field and modeling studies, *in* Wright, V.P., and Burchette, T.P., eds., Carbonate ramps: Geological Society of London Special Publication 149, p. 107–135.

Read, J.F., Grotzinger, J.P., Bova, J.A., and Koerschner, W.F., 1986, Models for generation of carbonate cycles: Geology, v. 14, p. 107–110, doi: 10.1130/0091-7613(1986)14<107:MFGOCC>2.0.CO;2.

Rice, W.D., and Langenheim, R.L., Jr., 1974a, Conodont zonation of the Battleship Wash Formation, Late Mississippian, Arrow Canyon Range, Clark County, Nevada: Wyoming Geological Association Earth Science Bulletin, v. 7, no. 2, p. 3–13.

Rice, W.D., and Langenheim, R.L., Jr., 1974b, Conodonts of the Battleship Wash Formation, Late Mississippian, Arrow Canyon Range, Clark County, Nevada: Wyoming Geological Association Earth Science Bulletin, v. 7, no. 2, p. 19–36.

Richards, B.C., Lane, R.H., and Brenckle, P.L., 2002, The IUGS Mid-Carboniferous (Mississippian-Pennsylvanian) global boundary stratotype section and point at Arrow Canyon, Nevada, USA, *in* Hills, L.V., et al., eds., Carboniferous and Permian of the world: Canadian Society of Petroleum Geologists Memoir 19, p. 802–831.

Rocha-Campos, A.C., dos Santos, P.R., and Canuto, J.R., 2008, Late Paleozoic glacial deposits of Brazil: Paraná Basin, *in* Fielding, C.R., et al, eds., Resolving the late Paleozoic ice age in time and space: Geological Society of America Special Paper 441, p. 97–114.

Ross, C.A., 1991, Pennsylvanian paleogeography of the western United States, *in* Cooper, J.D., and Stevens, C.H., eds., Paleozoic paleogeography of the western United States–II: Pacific Section, SEPM (Society for Sedimentary Geology) Publication 67, p. 137–148.

Ross, C.A., and Ross, J.R.P., 1987, Late Paleozoic sea level and depositional sequences: Cushman Foundation for Foraminiferal Research Special Publication 24, p. 137–149.

Royer, D.L., 1999, Depth to pedogenic carbonate horizon as a paleoprecipitation indicator?: Geology, v. 27, p. 1123–1126, doi: 10.1130/0091-7613(1999)027<1123:DTPCHA>2.3.CO;2.

Rygel, M.C., Fielding, C.R., Frank, T.D., and Birgenheier, L.P., 2008, The magnitude of late Paleozoic glacioeustatic fluctuations: A synthesis: Journal of Sedimentary Research, v. 78, p. 500–511, doi: 10.2110/jsr.2008.058.

Schenk, P.E., 1967, Facies and phases of the Altamont Limestone and megacyclothem (Pennsylvanian), Iowa to Oklahoma: Geological Society of America Bulletin, v. 78, p. 1369–1384, doi: 10.1130/0016-7606(1967)78[1369:FAPOTA]2.0.CO;2.

Sears, S.O., and Lucia, F.J., 1980, Dolomitization of northern Michigan Niagara Reefs by brine refluxion and freshwater/seawater mixing, *in* Zenger, D.H., et al., eds., Concepts and models of dolomitization: Society of Economic Paleontologists and Mineralogists Special Publication 28, p. 215–236.

Shinn, E.A., 1983, Tidal flat environment, *in* Scholle, P.A., et al., eds., Carbonate depositional environments: American Association of Petroleum Geologists Memoir 33, p. 172–210.

Smith, L.B., Jr., and Read, J.F., 2000, Rapid onset of late Paleozoic glaciation on Gondwana: Evidence from Upper Mississippian strata of the Midcontinent, United States: Geology, v. 28, p. 279–282, doi: 10.1130/0091-7613(2000)28<279:ROOLPG>2.0.CO;2.

Soreghan, G.S., and Dickinson, W.R., 1994, Genetic types of stratigraphic cycles controlled by eustasy: Geology, v. 22, p. 759–761, doi: 10.1130/0091-7613(1994)022<0759:GTOSCC>2.3.CO;2.

Soreghan, G.S., and Giles, K.A., 1999a, Amplitudes of Late Pennsylvanian glacioeustasy: Geology, v. 27, p. 255–258, doi: 10.1130/0091-7613(1999)027<0255:AOLPG>2.3.CO;2.

Soreghan, G.S., and Giles, K.A., 1999b, Facies character and stratal responses to accommodation in Pennsylvanian bioherms, western Orogrande Basin, New Mexico: Journal of Sedimentary Research, v. 69, p. 893–908.

Soreghan, G.S., Soreghan, M.J., Poulsen, C.J., Young, R.A., Eble, C.F., Sweet, D.E., and Davogustto, O.C., 2008, Anomalous cold in the Pangaean tropics: Geology, v. 36, p. 659–662, doi: 10.1130/G24822A.1.

Stamm, R.G., and Wardlaw, B.R., 2003, Conodont faunas of the late Middle Pennsylvanian (Desmoinesian) Lower Kittanning Cyclothem, U.S.A., *in* Cecil, C.B., and Edgar, N.T., eds., Climate controls on stratigraphy: SEPM (Society for Sedimentary Geology) Special Publication 77, p. 95–122.

Stanley, S.M., 2006, Effects of eustatic sea level lowering on terrestrial and shallow marine biotas: Geological Society of America Abstracts with Programs, v. 38, no.7, p. 337.

Stevens, C.H., and Stone, P., 2007, The Pennsylvanian–Early Permian Bird Spring carbonate shelf, southeastern California: Fusulinid biostratigraphy, paleogeographic evolution, and tectonic implications: Geological Society of America Special Paper 429, 82 p.

Stevens, C.H., Stone, P., and Belasky, P., 1991, Paleogeographic and structural significance of an Upper Mississippian facies boundary in southern Nevada and east-central California: Geological Society of America Bulletin, v. 103, p. 876–885, doi: 10.1130/0016-7606(1991)103<0876:PASSOA>2.3.CO;2.

Stevens, C.H., Stone, P., and Ritter, S.M., 2001, Conodont and fusulinid biostratigraphy and history of the Pennsylvanian to lower Permian Keeler Basin, east-central California: Brigham Young University Geology Studies, v. 46, p. 99–142.

Stollhofen, H., Werner, M., Stanistreet, I.G., and Armstrong, R.A., 2008, Single-zircon U-Pb dating of Carboniferous-Permian tuffs, Namibia, and the intercontinental deglaciation cycle framework, *in* Fielding, C.R., et al., eds., Resolving the late Paleozoic ice age in time and space: Geological Society of America Special Paper 441, p. 83–96.

Trexler, J.H., Jr., Snyder, W.S., Cashman, P.H., Gallegos, D.M., and Spinosa, C., 1991, Mississippian through Permian orogenesis in eastern Nevada: Post-Antler, pre-Sonoma tectonics of the western Cordillera, *in* Cooper, J.D., and Stevens, C.H., eds., Paleozoic paleogeography of the western United States–II: Pacific Section SEPM (Society for Sedimentary Geology) Special Publication 67, p. 317–330.

Trexler, J.H., Jr., Cole, J.C., and Cashman, P.H., 1996, Middle Devonian-Mississippian stratigraphy on and near the Nevada Test Site: Implications for hydrocarbon potential: American Association of Petroleum Geologists Bulletin, v. 80, p. 1736–1762.

Trexler, J.H., Jr., Cashman, P.H., Cole, J.C., Snyder, W.S., Tosdal, R.M., and Davydov, V.I., 2003, Widespread effects of Middle Mississippian deformation in the Great Basin of western North America: Geological Society of America Bulletin v. 115, p. 1278–1288, doi: 10.1130/B25176.1.

Trexler, J.H., Jr., Cashman, P.H., Snyder, W.S., and Davydov, V.I., 2004, Late Paleozoic tectonism in Nevada: Timing, kinematics, and tectonic significance: Geological Society of America Bulletin v. 116, p. 525–538, doi: 10.1130/B25295.1.

USGS, 1986, Arrow Canyon Quadrangle, Clark County, Nevada, 7.5 minute series topographic map: Reston, Virginia, USGS, Map number 36114-F7-TF-024.

Veevers, J.J., 1994, Pangea: Evolution of a supercontinent and its consequences for Earth's paleoclimate and sedimentary environments, *in* Klein, G. deV., ed., Pangea: Paleoclimate, tectonics, and sedimentation during accretion, zenith, and breakup of a supercontinent: Geological Society of America Special Paper 288, p. 13–23.

Veevers, J.J., and Powell, C.M., 1987, Late Paleozoic glacial episodes in Gondwanaland reflected in transgressive-regressive depositional sequences in Euramerica: Geological Society of America Bulletin, v. 98, p. 475–487, doi: 10.1130/0016-7606(1987)98<475:LPGEIG>2.0.CO;2.

Wanless, H.R., and Shepard, F.P., 1936, Sea-level and climatic changes related to late Paleozoic cycles: Geological Society of America Bulletin, v. 47, p. 1177–1206.

Wanless, H.R., and Weller, J.M., 1932, Correlation and extent of Pennsylvanian cyclothems: Geological Society of America Bulletin, v. 43, p. 1177–1206.

Webster, G.D., 1969, Chester through Derry conodonts and stratigraphy of northern Clark and southern Lincoln counties, Nevada: University of California Publications in Geological Sciences, v. 79, 121 p.

West, R.R., Archer, A.W., and Miller, K.B., 1997, The role of climate in stratigraphic patterns exhibited by late Palaeozoic rocks exposed in Kansas: Palaeogeography, Palaeoclimatology, Palaeoecology, v. 128, p. 1–16, doi: 10.1016/S0031-0182(97)81127-3.

Wilkinson, B.H., Drummond, C.N., Rothman, E.D., and Diedrich, N.W., 1997, Stratal order in peritidal carbonate sequences: Journal of Sedimentary Research, v. 67, p. 1068–1082.

Wilkinson, B.H., Diedrich, N.W., Drummond, C.N., and Rothman, E.D., 1998, Michigan hockey, meteoric precipitation, and rhythmicity of accumulation on peritidal carbonate platforms: Geological Society of America Bulletin, v. 110, p. 1075–1093, doi: 10.1130/0016-7606(1998)110<1075:MHMPAR>2.3.CO;2.

Wilson, J.L., 1967, Cyclic and reciprocal sedimentation in Virgilian strata of southern New Mexico: Geological Society of America Bulletin, v. 29, p. 5–34.

Wright, V.P., and Vanstone, S.D., 2001, Onset of late Paleozoic glacio-eustasy and the evolving climates of low latitude areas: a synthesis of current understanding: Geological Society of London Journal, v. 158, p. 579–582.

Yose, L.A., and Heller, P.L., 1989, Sea-level control of mixed-carbonate-siliciclastic, gravity-flow deposition: Lower part of the Keeler Canyon Formation (Pennsylvanian), southeastern California: Geological Society of America Bulletin, v. 101, p. 427–439, doi: 10.1130/0016-7606(1989)101<0427:SLCOMC>2.3.CO;2.

Zempolich, W.G., Cook, H.E., Zhemchuzhnikov, V.G., Zorin, A.Y., Giovannelli, A., Viaggi, M., Lehmann, P.J., Fretwell, N., Zhaimina, V.Y., Buvtyshkin, V.M., and Alexeiev, D.V., 2002, Biotic and abiotic influence on the stratigraphic architecture and diagenesis of middle to late Paleozoic carbonates of the Bolshoi Karatau Mountains, Kazakhstan and the southern Urals, Russia: Implications for the distribution of early marine cements and reservoir quality in subsurface reservoirs, *in* Zempolich, W.G., and Cook, H.E., eds., Paleozoic carbonates of the Commonwealth of Independent States (CIS): Subsurface reservoirs and outcrop analogs: SEPM (Society for Sedimentary Geology) Special Publication 74, p. 123–180.

Ziegler, A.M., Rees, P.M., and Naugolnykh, S.V., 2002, The Early Permian floras of Prince Edward Island, Canada: Differentiating global from local effects of climate change: Canadian Journal of Earth Sciences, v. 39, p. 223–238, doi: 10.1139/e01-075.

Manuscript Received 15 June 2008
Revised Manuscript Received 21 July 2009
Manuscript Accepted 13 August 2009